Constraints on the frequency and dispersal of explosive eruptions at Sambe and Daisen volcanoes (South-West Japan Arc) from the distal Lake Suigetsu record (SG06 core)

Paul G. Albert*[a], Victoria C. Smith[a], Takehiko Suzuki[b], Emma L. Tomlinson[c], Takeshi Nakagawa[d], Danielle McLean[a], Masataka Yamada[b], Richard A. Staff[e], Gordon Schlolaut[f], Keiji Takemura[g], Yoshitaka Nagahashi[h], Jun-Ichi Kimura[i], Suigetsu 2006 Project Members.

**Corresponding author*

[a] *Research Laboratory for Archaeology and the History of Art, University of Oxford, Oxford, OX1 3QY, United Kingdom*

[b] *Department of Geography, Tokyo Metropolitan University, Minamiosawa, Hachioji, Tokyo, Japan*

[c] *Department of Geology, Trinity College Dublin, Dublin 2, Ireland*

[d] *Research Centre for Palaeoclimatology, Ritsumeikan University, Kyoto, 603-8577, Japan*

[e] *Scottish Universities Environmental Research Centre, University of Glasgow, Scotland*

[f] *Centre for Ocean Science Drilling, Japan Agency for Marine-Earth Science Technology, Yokohama, Japan*

[g] *Institute for Geothermal Science, Kyoto University, Kyoto, 606-8502, Japan.*

[h] *Faculty of symbiotic Systems Science, Fukushima University, 1 Kanayagawa, Fukushima 960-1296, Japan*

[i] *Department of Solid Earth Geochemistry, Japan Agency for Marine-Earth Science and Technology, Yokosuka 237-0061, Japan*

Abstract:

Accurately evaluating the tempo and magnitude of pre-historic eruptions is essential for hazard assessments. Here we demonstrate the importance of integrating records from locations close to the volcano with those in distal regions to generate more comprehensive event stratigraphies. The annually laminated (varved) and intensely radiocarbon dated lacustrine sediments of Lake Suigetsu (SG06 core), Japan are used to place chronological constraints on the tempo of volcanism at two stratovolcanoes located favourably upwind of the lake along the South-West Japan Arc, Sambe and Daisen. Major and trace element glass compositions are used to assign visible ash (tephra) layers preserved in the SG06 sediment core to past explosive eruptions from these volcanoes. Integrating these stratigraphies confirm that the ~150 ka long lake sequence records nine visible ash layers from Daisen and five from Sambe. The SG06 record captures two periods of closely spaced eruptions at Daisen volcano. The first period begins at ~61.9 ka with three explosive eruptions over ~10 ka, with two events separated by as little as 1.5 ka. One layer (SG06-4281), dated at 59.6 ± 5.4 ka (95.4% probability), relates to the large magnitude, and widely dispersed Daisen Kurayoshi Pumice (DKP) eruption. The other period of frequent activity began at 29,837 ± 96 IntCal13 yrs BP (95.4% probability) with five widely dispersed ash fall events associated with explosive eruptions separated by approximately 6, 936, 5 and 438 years. The integrated proximal-distal event stratigraphy and the high-precision SG06 chronology provide unique insights into the timing and frequency of past explosive volcanism from Daisen and Sambe, which has implications for the prediction of future eruption scenarios.

Key words: Eruption frequency; Daisen; Sambe; Lake Suigetsu (SG06 core); South-west Japan Arc (SWJA); High-precision Tephrochronology.

1. Introduction

Reconstructing the eruptive history of a volcano is essential for assessment of hazards and risk associated with future activity. In proximal settings, close to the volcano, it can be challenging to reliably elucidate the true volcanic history due to incomplete or patchy exposures, often owing to the burial or destruction of older deposits by younger explosive activities, but also due to poor preservation or high rates of pedogenesis. These complexities mean even well-studied Quaternary volcanic records, including those included in Japanese databases (e.g., Machida and Arai, 2003), underestimate the number of volcanic eruptions, which has obvious implications for hazard assessments (Kiyosugi et al., 2015).

Volcanic ash (tephra) layers recorded in distal lacustrine sedimentary archives have proven increasingly important for building more detailed inventories of past explosive activity of volcanic regions (e.g., Wulf et al., 2004; 2012; de Fontaine et al., 2007; Wastegard et al., 2013; Smith et al., 2013; Tomlinson et al., 2014; Giaccio et al., 2017), these tephra repositories offer crucial insights into the dispersal of volcanic ash associated with individual eruptions along with their magnitude. This information is increasingly being used to inform future eruptive scenarios and hazard assessments (e.g., Shane and Hoverd 2002; Sulpizio et al., 2014). Owing to the independent dating of lacustrine sedimentary records (e.g, radiocarbon, varve chronologies) they can offer unique insights into the timing and tempo of past volcanism across a region or for specific volcanoes (e.g., Wulf et al., 2004; Albert et al., 2013; Smith et al., 2013; Tomlinson et al., 2014).

Here we utilise the tephra layers preserved in the high-resolution lacustrine sediments of Lake Suigetsu (SG06 core), Honshu Island, Japan (**Fig. 1**), which span approximately the last 150 ka (Nakagawa et al., 2012) to reconstruct the eruptive activity of the largest stratovolcanoes situated on SW Honshu and associated with subduction along the South West Japan Arc (SWJA), Mt. Sambe and Mt. Daisen. Both centres active during the Late Quaternary are characterised by lava dome extrusion and siliic pyroclastic material which is generally dacitic in composition (Morris, 1995). The last large (Volcanic Explosivity Index [VEI] 5) eruption at Sambe is dated to have occurred between 3,985-4,085 IntCal13 yrs BP (**Table 1**), whilst Daisen has been quiescent during the Holocene and its last activity is dated at between 20,635-21,015 IntCal13 yrs BP (**Table 1**). Due to the prevailing westerlies, Lake Suigetsu is ideally situated downwind of these two volcanoes and thus should preserve a detailed eruption event stratigraphy. The sediments of the SG06 record which span the last 50 ka, have been subject to intense radiocarbon dating (Staff et al., 2011; Bronk Ramsey et al., 2012), and they are annually laminated (varved) between 10-50 ka, thus offering an unrivalled chronology (Bronk-Ramsey et al., 2012) capable of better constraining the explosive eruption histories of Sambe and Daisen.

The explosively erupted products of Sambe (e.g., Fukuoka and Matsui, 2002; Machida and Arai, 2003) and Daisen (e.g., Machida and Aira, 1979; 2003; Tsukui, 1984; Okada and Ishiga, 2000; Kato et al. 2004, Furusawa, 2008; Yamamoto, 2017), have been subject to detailed stratigraphic proximal reconstructions, yet inconsistencies exist between the interpretations of their volcanic histories, and seemingly the frequency of recorded events decreases further back in time. Table 1 presents the most widely accepted reconstructions of the recorded major explosive eruptions of these two volcanoes. The pyroclastic deposits on the slopes of these volcanoes are often heavily weathered (e.g., Furusawa, 2008) and consequently, only limited volcanic glass data is available for their eruptive products (e.g.,

Kimura et al., 2015). Much of the existing data is of melt inclusions rather than matrix glass (e.g., Furusawa, 2008), which is not ideal for geochemical correlations.

Thirty-one visible ash layers were identified in the sediments of the SG06 record (Smith et al. 2013; McLean et al. 2016). Major element glass analysis revealed that twenty-nine low-K tholeiitic, through to medium-K calc-alkaline (CA) and High-K calc-alkaline (HKCA) tephra layers are derived from volcanic sources along the Japanese arc (Smith et al., 2013; **Fig. 2**). These tephra layers range in composition from basalt through to rhyolite, with more evolved compositions dominating. The glass chemistries of some tephra layers significantly overlap at a major element level. Some of the thickest tephra layers in the SG06 record have been linked to large caldera-forming eruptions in and around Kyushu Island using their major element compositions and these include important and widespread Japanese tephrostratigraphy markers such as the Kikai-Akahoya (K-Ah; SG06-0967), Aira-Tanzawa (AT; SG06-2650), Aso-4 (SG06-4963), Kikai Tozurahara (K-Tz; SG06-5181) and Ata (SG06-5353) (Smith et al., 2013). Many of the remaining SG06 tephra layers could not be attributed to a proximal source owing to the paucity of available proximal volcanic glass data and the overlapping major element glass chemistries produced by many of the Japanese volcanoes (**Fig. 2**).

In this contribution we examine the trace element compositions of the volcanic glasses from twenty-three of the thirty-one visible tephra layers previously reported in the SG06 record in an attempt to determine those derived from explosive activity at Sambe and Daisen. To achieve this, the trace element signatures of the distal SG06 tephra layers were compared to new proximal reference glass data generated from the eruptive products sampled at these two volcanic sources. The SG06 layers were also compared to the known trace element compositions of tephra units erupted from the large calderas of southern Kyushu, northern Honshu and Hokkaido, and the stratovolcanoes of the Norikura volcanic zone (Kimura et al., 2015; Maruyama et al., 2016).

The trace element glass chemistry allows some of the SG06 tephra layers to be assigned to explosive volcanism along the SWJA, and the existing and new major element glass data from the distal layers and proximal deposits are used to link these to specific eruptions. We also compare the SG06 Sambe and Daisen derived layers to those previously reported in other important sedimentary records including Lake Biwa (Takemura et al., 2010; Kigoshi et al., 2014), Ichi-no-Megata (Okuno et al., 2011) and the Sea of Japan (Domitsu et al., 2002; Ikehara et al., 2004; 2015; **Fig. 1**) to get a better grasp of the complete event stratigraphy and individual ash dispersals. The SG06 stratigraphic record and chronology elucidates the tempo of explosive activity at Sambe and Daisen, whilst also gleaning new insights into the chemical evolution of the two volcanic systems.

2. Methods

2.1 Electron microprobe (EMP)

Major and minor element volcanic glass chemistry of individual juvenile clasts was determined using a wavelength-dispersive JEOL 8600 electron microprobe in the Research Laboratory for Archaeology and the History of Art, University of Oxford. A beam accelerating voltage of 15kV was used with a 6nA current and a beam diameter of 10 µm. The instrument was calibrated with a suite of appropriate mineral standards; peak count times were 30 s for

all elements except Mn (40s), Na (12s), Cl (50s) and P (60s). Reference glasses from the Max Plank institute (MPI-DING suite; Jochum et al., 2006) bracketing the possible chemistries were also analysed alongside the unknown volcanic glasses. These included felsic (ATHO-G rhyolite), through intermediate (StHs6/80-G andesite) to mafic (GOR128-G komatiite) glasses. All glass data has been normalised to 100 % for comparative purposes. This is of paramount importance for tephras in marine and lacustrine cores, as glass shards may absorb water from their surroundings, which often results in low totals. Analytical totals < 93% were discarded. Errors are typically < ± 0.7% relative standard deviation (RSD) for Si; ~ ± 3% for most other major elements, except for the low abundance elements like Ti (~ ± 7%) and Mn (~ ± 30%). Error bars on plots represent reproducibility, calculated as a 2 x standard deviation of replicate analysis of MPI-DING StHs6/80-G. Glass standard data are reported in **Supplementary Material 1** along with the full geochemical data sets.

2.2 Laser Ablation Inductively Coupled Plasma Mass Spectrometry (LA-ICP-MS)

The analyses were performed using a Thermo Scientific iCAP Qc ICP-MS coupled to a Teledyne Photon Machines Analyte G2 193 nm eximer laser ablation system with a HelEx II two-volume ablation cell at the Department of Geology, Trinity College, Dublin. Spot sizes of 30, 25 and 20 µm were used owing to varying size of the ash particles and glassy areas available for analysis. The repetition rate was 5 Hz and the count time was 40 s (200 pulses) on the sample and 40 s on the gas blank (background). The ablated sample was transported in He gas flow (0.65 L min^{-1}) with additional N_2 (5 ml min^{-1}) via a signal smoothing device. Concentrations were calibrated using NIST612 with ^{29}Si as the internal standard and using a Ca correction factor as advocated in Tomlinson et al. (2010). Data reduction was performed using Iolite 2.5 and portions of the signal compromised by the ablation of microcrysts and resin-filled voids were excluded. Accuracies of ATHO-G and StHs6/80-G MPI-DING glass analyses are typically ≤5% for V, Rb, Sr, Y, Zr, Ba, La, Ce, Nd, Eu, Dy, Er, Th; <10% for Nb, Pr, Sm, Gd, Yb, Hf, U and <15% for Ta. Reproducibility of the ATHO-G analyses were typically < 5% RSD for all trace elements with the exception of Sm, Eu, Yb (<6%) and V (≤8%). Analyses of MPI-DING secondary standards are provided in the **supplementary material 1** along with the full data sets.

2.3 Chronology

The SG06 sedimentary record is underpinned by the chronology presented in Bronk Ramsey et al. (2012), which provides an integral component of the current International Radiocarbon (^{14}C) Calibration (IntCal) dataset (Reimer et al., 2013). The independent chronology of the Lake Suigetsu SG06 sedimentary sequence has subsequently been age-depth modelled on to the IntCal13 timescale implementing three successive cross-referenced Poisson-process (*'P_Sequence'*) depositional models using OxCal (ver. 4.3; Bronk Ramsey 2008; 2017). These include 775 AMS ^{14}C dates obtained from terrestrial plant macrofossils from the upper 38 m (SG06-CD) of the SG93 and SG06 sediment cores (Kitagawa and van der Plicht, 1998a, 1998b, 2000; Staff et al., 2011, 2013a, 2013b) and varve counting between 12.88 and 31.67m SG06 CD (Marshall et al. 2012; Schlolaut et al. 2012). Ages for core depths of identified tephra deposits were generated using the '*Date'* function and differential ages between these dated tephra were calculated using the '*Difference*' function in OxCal. All ^{14}C ages presented in this paper, including those from published literature (eruption ages), have been calibrated using IntCal13 and are reported as 'IntCal13 yrs BP' with the 95.4% probability range (equivalent to 2σ error). The IntCal13 Suigetsu chronology has also been

transferred to a new SG14 sedimentary profile using 361 common marker layers throughout the sedimentary sequence.. Beyond the annually laminated and ^{14}C dated portion of the sequence, the age-depth model is based on a linear extrapolation that is anchored by deeper chronological tie points (Staff et al., 2013a), which include $^{40}Ar/^{39}Ar$ ages of volcanic units (e.g., Aso-4/SG06-4963). All ages reported that are outside the ^{14}C timeframe are provided in ka with 2σ errors (equivalent to 95.4% probability range). Placing the SG06 chronology onto the IntCal13 timescale allows its direct comparison with other ^{14}C dated deposits and records that are calibrated using IntCal13. Published proximal ^{14}C dates from charcoal fragments were re-calibrated here using IntCal13. Where multiple proximal ^{14}C ages were available from a single eruption deposit these were combined and calibrated in an OxCal model using IntCal13.

2.4 Proximal reference volcanic glasses

Fresh proximal pumice and ash samples from explosive eruptions of both Sambe and Daisen volcanoes were analysed to generate a reference volcanic glass dataset suitable for deciphering the provenance of SG06 tephra layers and assessing eruption specific correlations. Eruptive units from Sambe (**Table 1**) characterised here, from youngest to oldest, based on existing stratigraphic interpretations, are the: Taiheizan pyroclastic flows (Th-pfl), Shigaku pyroclastic flows (S2-fl), Kiriwari ash fall (Kr-fa), Ukinuno ash fall (Uk-fa), Midorigaoka pyroclastic flow (Md-fl), Ukinuno pumice fall (Uk-pfa/U2), Oda pumice flow or SUk flow (Od-fl/U1), Hatasedani pyroclastic flow (Ht-fl), Ikeda Pumice fall (SI or Ik-pfa), Oda pumice flow (SOd) and Unnan pumice fall (SUn). These Sambe samples broadly follow the sampling, nomenclature and stratigraphy presented in Fukuoka and Matsui (2002; and references therein). Extremely poor preservation of eruptive units at Daisen volcano prohibited geochemical characterisation of all the thick eruptive units reported (**Table 1**). We were able to characterise proximal glass data from the following eruptions (youngest to oldest): Daisen Katsatanihara pumice fall (DKs), Higashi-daisen pumice fall (DHg), Daisen Sasaganaru pyroclastic flows (DSs), and finally pumices fragments, thought to be associated with the Daisen Sekigane Pumice (DSP). These samples follow the stratigraphy, nomenclature and sampling of Machida and Arai (2003). Details of all proximal samples, including localities and glass compositions can be found in **Supplementary material 1**.

3. Results

Volcanic glasses from thirteen of the twenty-three SG06 CA to HKCA (**Fig. 2a-b**) tephra layers analysed using LA-ICP-MS **(Table 2-3)** have trace element, multi-element signatures consistent with glasses from proximal deposits erupted at Sambe and Daisen stratovolcanoes situated on the SWJA (**Fig. 2C-F**). Trace element concentrations normalised to Primitive Mantle compositions (Sun and McDonough, 1989) reveal overall enrichments in incompatible trace elements, including the large ion-lithophile elements (eg., Rb), and depletions in Nb and Ta consistent with their arc origin (**Fig. 2C-F**). Mantle normalised profiles of these volcanic glasses are depleted in the middle and heavy rare earth elements (REE), when compared to all other portions of the Japanese arc, this is manifested in their steeper overall profiles **(Fig. 2C-F)**. These depletions in the middle to heavy REE mean that concentrations of these elements were often below the analytical detection limits in many glass shards. Fortunately, higher absolute concentrations of Y offer an important diagnostic tool for assigning tephra layers in the SG06 record to SWJA volcanism. Low Y (<10 ppm) concentrations are a feature considered unique to this particular Japanese arc (e.g., Kimura

et al., 2015) (**Fig. 2C-F; Fig. 3**), thus plotting the yttrium content of the SG06 tephra layers against core depth we can immediately build a record of ash fall events likely to derive from explosive volcanism along the SWJA. Those tephra layers displaying more elevated Y contents (>10 ppm) are not from volcanoes along the SWJA and are not discussed further here (**Fig. 3**).

Geochemically deciphering the eruptive products of Sambe and Daisen is more challenging owing to the overlapping concentrations of many major, minor and trace elements (e.g., **Fig 4; Fig. 5**). Proximal glass data plotted on a SiO_2 vs CaO diagram reveals that the Sambe and Daisen glasses reside on two separate evolutionary trends (**Fig. 4C**), where volcanic glasses erupted at the former are typically more enriched in CaO at a given SiO_2 content relative to those of the latter. Above 76 wt.% SiO_2 this feature becomes poorly defined, and some Sambe glasses drop to significantly lower CaO content (accompanied by an increase in K_2O), whilst the CaO content in Daisen glasses does not continue to decrease with increasing SiO_2, therefore leading to a convergence of the two compositional arrays (**Fig. 4C**). Plotting the SG06 layers assigned to the SWJA on a SiO_2 vs. CaO plot therefore is the first order means of geochemically assigning volcanic source (**Fig. 4C**). Where the distal tephra is dominated by SiO_2 contents > 76 wt.%, the observed trend to less evolved compositions is often diagnostic of volcanic source (**Fig. 4C; Supplementary Fig. 1**). Whilst, incompatible trace element concentrations do not enable easy distinction between Sambe and Daisen tephra deposits (**Fig. 5**), the proximal reference glasses analysed do reveal that those erupted from the Sambe are typically more depleted in Zr. This greater depletion in Zr is best illustrated by lower Zr/Th ratios in the Sambe glasses relative to those of Daisen (**Fig. 4G**).

Of the thirteen SG06 layers initially assigned here to volcanism along the SWJA **(Table 2)**, four tephra layers have either a CaO (vs. SiO_2) content or Zr/Th ratio more consistent with melt compositions from proximal Sambe volcano reference glasses (**Fig. 4; Supplementary Fig.1**). Two of these Sambe derived layers occur above the AT tephra (SG06-0588 and SG06-1965) and the other two lie stratigraphically below the AT tephra (SG06-3688 and SG06-4124).

Four tephra layers stratigraphically above the AT marker demonstrate lower CaO content (vs.SiO_2) or higher Zr/Th ratios consistent with glasses erupted at Daisen volcano (SG06-2504, SG06- 2534, SG06-2601 and SG06-2602; **Fig. 4; Supplementary Fig.1**). A fifth previously un-reported layer (SG06-2535; **Table 2**), characterised at a major element level, is geochemically identical to overlying SG06-2534 tephra and thus from Daisen (**Fig. 4**). Below the AT marker two tephra layers (SG06-4281 and SG06-4318) show compositions consistent with proximal Daisen reference glasses (**Fig. 4; Supplementary Fig.1**). A further three SWJA tephra layers beneath the AT tephra remain more difficult to assign specifically to either Sambe or Daisen based on glass chemistry alone (SG06-3974, SG06-4141 and SG06-6457) and the tephrostratigraphy in both the proximal and distal (SG06) settings must be considered.

4. Discussion

In the following sections we explore the eruption specific tephra correlations between the SG06 tephra layers and eruptions from Sambe and Daisen volcanoes that are known from previous logging and mapping of proximal deposits (**Table 1**). This enables us to establish a

fully integrated proximal-distal eruption stratigraphy for these volcanoes. Tephra correlations are discussed based on their stratigraphic positions relative to Aira Tanzawa (AT) tephrostratigraphic marker, prominent in the stratigraphies of both volcanoes (**Table 1**) and the SG06 record (SG06-2650).

4.1 SG06 - Sambe tephra correlations

4.1.1 Post-AT activity

The youngest layer in SG06 attributed to Sambe is the Holocene tephra SG06-0588 which is dated at 4,004-4,068 IntCal13 yrs BP (95.4%). The glass compositions of this CA to HKCA tephra are consistent with proximal glasses of the Taiheizan (Th-pd) block and ash flow also known as the Sambe Ohirasan (SOh) tephra (**Fig. 6A-B**; **Table 1**). Charcoals buried in this eruptive deposit have been ^{14}C dated (Fukuoka and Matsui, 2002; and reference therein) and these ^{14}C ages have been combined (OxCal) and recalibrated to date the eruption between 3,895-4,085 IntCal13 yrs BP (95.4%; **Table 1**), which is consistent with the SG06-0588 layer (**Supplementary Fig. 2A**). Stratigraphically below SG06-0588 in the Holocene sediments, McLean et al. (2018), identify a second layer SG06-0775 (= SG14-0781) with a broadly overlapping major element composition to the younger SG06-0588/Taiheizan tephra. SG14-0781/SG06-0775 is dated at 5,481-5,521 IntCal13 yrs BP (95.4%), and is compositionally consistent with the Shigaku pyroclastic flow deposits (S2-fl), which show slightly lower K_2O contents than the Taiheizan glasses (**Fig. 5 A-B**). Proximal charcoal ^{14}C ages (modelled in OxCal) reveal that the pyroclastic flow occurred between 5,330-5,590 IntCal13 yrs BP (95.4%; **Table 1**), which is in strong statistical agreement with the Lake Suigetsu tephra age (**Supplementary Fig. 2A)**.

The CA to HKCA SG06-1965 tephra dated at between 19,471-19,631 IntCal13 yrs BP (95.4%) is compared to glass data from eruptive deposits associated with explosive activity occurring at Sambe at the end of the last glacial (Cycle IV; **Table 1**). These units are stratigraphically bracketed by an upper palaesol (the 4th black soil), ^{14}C dated at between 12,690-12,875 IntCal13 yrs BP (95.%) and an underlying palaeosol containing AT glasses (Fukuoka and Matsui, 2002; Matsui and Fukuoka, 2003). Proximally, this explosive activity comprises the widespread Sambe tephra fallout, the Ukinuno pumice (SUP/SUk) as described by Machida and Arai (2002), with its mapped ESE dispersal (>200 km). Fukuoka and Matsui, (2002) describe a more complex succession of eruptive units at source, the more prominent Ukinuno pumice is divided into two units a lower 'Oda'/'Unit 1' flow (Oda-fl) deposit and an upper Ukinuno sub-Plinian fall/'Unit 2' (Uk-pfa; **Table 1**). Multiple charcoal ^{14}C ages were combined (OxCal) to give an age of 19,050-19,445 IntCal13 yrs BP (95.4%) for the Oda fl (**Table 1**). Fukuoka and Matsui, (2002) resolve two additional pyroclastic flow units, Midorigaoka (Mt-fl; 19 ± 4 ka [Thermal Luminescence] ; **Table 1**) and Hatasedani (Ht-fl; 18,880-20,790 IntCal13 yrs BP (95.4%); **Table 1**), and place them above and below the Unit 1-2 deposits respectively, illustrating a complex period of explosive activity at Sambe volcano.

Away from source, distal ash associated with this period of activity is reported across northern and southern Kinki District and is known as the '*Sakate'* tephra (Katoh et al., 2007), named after its discovery at Sakate in the Nara Basin (Ooi, 1992), over 250 km south-east of Sambe. It is also recognised in the sediments of Lake Biwa (BT6; Yoshikawa and Inouchi, 1991). Here we consider new glass data from Lake Biwa tephra layer BIW07-06- 5.59 m

which is ascribed as Sakate tephra (**Table 4;** Takemura et al., 2010; Kigoshi et al., 2014). Typically the Sakate distal ash layers are thought to be associated with the SUP/UK-pfa (sub-Plinain) eruption deposits, however discrepancies in heavy mineral componentry (cummingtonite abundance) and refractive indices between proximal and distal units, lead some authors to suggest an alternative correlation to the underlying Oda-fl/Unit 1 (see Katoh et al., 2007).

Glass chemistry here reveals unequivocally that the sub-Plinian Ukinuno pumice fall (Uk-pfa/Unit 2) does not display the full compositional range of the distal SG06-1965 tephra or the Lake Biwa Sakate ash layer (**Fig. 6C-D**). Ukinuno pumice fall glasses are less evolved, with lower SiO_2 and K_2O (**Fig. 6C**), and higher CaO and FeOt contents (**Fig. 6D**). Whilst the stratigraphically lower Oda flow (Unit 1) and Hatesedani flow deposits extend to higher SiO_2 contents that are consistent with the SG06-1965 glasses (**Fig. 6C**), the former are offset to higher FeOt (**Fig. 6D**) and the latter are restricted to lower K_2O contents at overlapping SiO_2 (**Fig. 6C**). The only proximal unit associated with this period of explosive activity at Sambe to precisely match the glass composition of SG06-1965 (and the widespread distal Sakate tephra layer) is the Midorigaoka Ash flow deposits that are exposed south of the summit area, crucially these glasses show identically low FeOt and higher K_2O contents consistent with the distal ash dispersal **(Fig., 6C-D)**. This correlation causes a chrono-stratigraphic discrepancy at volcanic source as Fukuoka and Matsui, (2002) place the Midorigaoka ash flow (Md-fl) above the Oda-fl (Unit 1; 19,050-19,445 cal yrs BP [95.4%]), yet the distal age of the Migorigaoka Ash Flow/SG06-1965 is marginally older (19,471-19,631 IntCal13 yrs BP [95.4%]; **Table 2; Supplementary Fig. 2B**), whilst also being consistent with the age of the Hatesedani flow (Ht-fl). The strong geochemical link between the Midorigaoka ash flow (Md-fl) deposits and SG06-1965/Sakate should provoke reassessment of the stratigraphic ordering of eruptive events at localities around the volcano.

4.1.2 Pre-AT activity

Trace element glass data reveals that SG06-3668 dated at 45,877-46,713 IntCal13 yrs BP (95.4%) relates to Sambe on the basis of its low Y content, coupled with a low Zr/Th ratio (**Fig. 3B**). This distal tephra layer also contains volcanic glasses from a non-SWJA source, as reflected by their high-Y (**Fig. 3**) and FeOt contents (**Fig**. **6E-F),** suggesting that two volcanoes erupted simultaneously or within a few months of each other.

Chronologically, the SG06-3668 layer is broadly consistent with the reported age of the Sambe Ikeda (SI) Plinian eruption (Machida and Aria, 2003; **Table 1**). Proximal SI fall reference deposits from a selection of localities around Sambe (**Supplementary material 1**) reveal significant heterogeneity in the major element glass compositions, as best reflected in variations in K_2O (**Fig. 6E-F**). Some of the SI proximal deposits are consistent with younger activity at the volcano (Cycles IV-VII; **Fig. 6**), with a clear CA affinity, whilst others are more enriched in K_2O content with a HKCA affinity, more consistent with the older eruptions at Sambe (**Fig. 6E**). SG06-3668 show some overlap with the proximal SI fall deposits, whilst the majority appear to represent mixing between the two dominant geochemical end-members in the proximal SI glasses (**Fig., 6F**). The absence of the hybrid compositions proximally is peculiar as chrono-stratigraphic evidence would suggest that SG06-3668 relates to the Plinian activities of SI. We tentatively correlate SG06-3668 with the proximal SI.

Major element glass data of the Lake Biwa tephra BIW07-06-16.02-16.04 m ascribed to Sambe Ikeda (SI) (Takemura, et al., 2010; Kigoshi et al., 2014) is far less heterogeneous at a major element level (**Table 4**) than the SI proximal deposit, but it has compositions that overlap with SG06-3668 tephra layer (**Fig**. **6E-F)**. Conversely, trace element data from the Lake Biwa tephra reveals a bi-modality, some glasses are consistent with the SG06-3668 glasses in terms of their levels of incompatible trace element enrichment (e.g., Th content), whilst the remaining glasses are far less enriched in incompatible trace elements and instead are similar to the magmas erupted during older activity of the volcano (Cycles I-II; **Fig**. **6G-H)**. This trace element bi-modality is an unusual feature as it is not observed in the major element glass data, with the absence of higher K_2O glasses associated with the older eruptions from the volcano and the less enriched incompatible trace element concentrations. It is possible that these high K_2O glasses were just not analysed at a major element level (**Table 4**). Overall the geochemical data presented here would indicate that SG06-3668 and tephra BIW07-06-16.02-16.04 m relate to the same ash dispersal.

Moving deeper into the SG06 record and beyond the varved portion of the core there is another tephra that has glass compositions consistent with a Sambe origin. The SG06-4124 tephra layer glasses display low Y contents and low Zr/Th ratios consistent with Sambe activity (**Fig. 6G-H**). These distal volcanic glasses show lower levels of incompatible trace element enrichment consistent with older eruptive activity in Cycles II (Unnan and Oda) and I (Kisuki) (**Table 1; Fig. 6G-H**). The SG06-4124 tephra displays enriched K_2O contents that are inconsistent with the younger Sambe tephra deposits **(Fig. 6)**. The SG06 age-depth model yields an age of 53.8 ± 1.0 ka (95.4 %) for SG06-4124. This age is chrono-stratigraphically consistent with activities of eruptive cycle II at Sambe (**Table 1**), and the major and trace element glass composition of SG06-4124 precisely match those of the Sambe Unnan (SUn) fall deposits. Whilst the trace element compositions of Sambe Oda (SOd) and SUn are incredibly similar, the major element data suggests slightly better agreement between SG06-4124 and the Plinian fall of SUn, as both proximal and distal glasses extend to lower K_2O content than those observed in the SOd flow deposits (**Fig. 6E**).

4.2 Daisen tephra correlations

4.2.1 Post-AT activity

Immediately above the AT tephra in the Lake Suigetsu stratigraphy is a succession of five HKCA (**Fig. 7**) Daisen derived tephra layers (SG06-2602; SG06-2601; SG06-2535, SG06-2534 and SG06-2504) as identified based on their major and trace element affinities. These five Daisen tephra layers span a short time interval between 29,935-28,370 IntCal13 yrs BP (95.4%). In the proximal setting above the AT ash layer, numerous tephrostratigraphic schemes are depicted (Table 1; Machida and Arai, 1979, 2003; Tusuki, 1984; Miura and Hayashi, 1991; Okada and Ishiga; 2000; Kimura et al., 2005; Yamamoto, 2017). It is generally accepted that the first post-AT activity is comprised of minor fallout and flows associated with the Vulcanian activity of Daisen Sasaganaru (DSs), as named by Machida and Arai (2003). DSs has been more recently sub-divided into three separate units (**Table 1**), the early Sasaganaru ash fall (SaA) and the more voluminous Sasaganaru flows (SaF; **Table 1**), distributed largely to the east of the volcano, and then fallout from further Vulcanian activity that is named the Odori (OdA) (Kimura et al., 2005; **Table 1**). The OdA is found on a thin humic soil, which suggests a time break or an eruption hiatus (Kimura et al., 2005). DSs pumices were analysed from flow deposits east of the volcano (**Supplementary**

material 1), major element analyses reveal these HKCA glasses are entirely consistent with those of both SG06-2602 and SG06-2601 tephra layers preserved in the Lake Suigetsu record (**Fig. 7A**). SG06-2601 glasses do extend to more evolved glass compositions (e.g., higher SiO_2), but these glasses are largely attributed to an additional background component of AT glass shards (**Fig. 7**). Trace element data comparisons between the DSs proximal deposits and both SG06-2602 and SG06-2601 reveal near identical glass compositions (**Fig. 5**) and consistent homogeneous trace element ratios (**Fig. 7D**), which suggests that the two layers in Lake Suigetsu directly above AT represent the distal equivalents of the lower voluminous DSs flow deposits (SaF; Table 1) and the Odori ash fall (OdA; **Table 1**). Similarly two layers immediately above AT in the Lake Biwa core BIW07-06 (Takemura et al., 2010; Kigoshi et al., 2014), 9.370-9.375m and 9.380-9.385m, previously assigned to DSs and re-analysed here (**Table 4**), are compositionally identical to SG06-2602 and SG06-2601 (**Fig. 7C**). Therefore, both Lake Suigetsu (SG06) and Lake Biwa sedimentary records confirm an eruption hiatus between two widespread eruption phases.

The SG06-2535, SG06-2534 and SG06-2504 layers all have major element compositions that overlap with the two older post-AT Daisen layers **(Fig. 7)**. The glass compositions of SG06-2535 and SG06-2534 predominantly extend to more elevated SiO_2 than the SG06-2602/2601 glasses (**Fig. 7**), beyond the SiO_2 content of the proximal DSs glasses and consistent with the most evolved glasses of the younger Higashi-daisen (DHg) and Kusadanihara (DKs) fall units (**Fig. 7**). The uppermost Daisen layer, SG06-2504, is more heterogeneous in its major element composition than the underlying layers, the most silicic end-member glasses are again reworked AT glass shards (**Fig., 7**). At a trace element level, both SG06-2534 and SG06-2504 tephra layers show overlapping concentrations when compared to the underlying Daisen SG06 layers, but are more variable, which is best illustrated by their range in Y and Zr content (**Fig. 5**). Consequently, whilst Zr/Th and Y/Th ratios overlap with the DSs proximal glasses, reinforcing their Daisen attribution, their greater variability demonstrates they are inconsistent with the more homogeneous DSs eruptive deposits **(Fig. 7D)**.

The tephra layers (SG06-2535, SG06-2534, SG06-2504) above the two DSs layers (SG06-2602/SG06-2601) in Lake Suigetsu are more difficult to link to specific Daisen tephra units owing to differing published proximal eruption stratigraphies (**Table 1**), and the deposits are often too poorly preserved for detailed geochemical analysis (Kimura et al., 2005). Poor glass preservation due to weathering has restricted the number of analyses from the Hagashi-daisen fall (DHg) (**Supplementary material 1**), and the Masumizhara flow (MsP) deposits, associated with the collapse of the Misen dome (Yamamoto, 2017), could not be characterised.

The SG06-2535 and SG06-2534 glasses extend to higher SiO_2 contents than those of DSs proximal glasses, and are consistent with both the evolved end-members of the DHg and stratigraphically younger DKs tephra **(Fig. 7),** but the latter can be excluded as a correlative on chronological grounds (**Table 1**). The Daisen component of SG06-2504 (i.e., excluding reworked AT glasses) are broadly less evolved than SG06-2535 and SG06-2534 glasses, but overlap with the less evolved DHg glasses (**Fig. 7**). Therefore, geochemistry alone indicates that SG06-2535, SG06-2534 or SG06-2504 could all be related to the DHg activities. However, the MsP is dated at between 28,041-28,628 IntCal13 yrs BP [95.4%] (**Table 1**) and is chronologically too young to be related to either the SG06-2535 or SG06-2534 tephra layers in the Lake Suigetsu record (**Supplementary Fig. 2**). The age of SG06-

2504 (28,449 ± 78 cal yrs BP [95.4%]) is however in very good statistical agreement with the age of the MsP pyroclastic flow (**Supplementary Fig. 2; Table 1**).

In summary based on the chemical similarity between SG06-2535, SG06-2534 and proximal DHg glasses, and proximal chronological constraints, SG06-2535 and SG06-2534 are both assigned to DHg activity and SG06-2504 to the younger MsP (**Fig. 7**). Detailed proximal investigations by Kimura et al., (2005) suggested a stratigraphic sub-division of the Higashi-daisen eruptive unit on the basis of an erosional unconformity separating the opening ash fall unit (HgA) from the overlying sub-Plinian/Plinian pumice fall deposits (HgP). The presence of two closely spaced tephra layers in the SG06 record (SG06-2535 and SG06-2534) with identical compositions to the Higashi-daisen pumices would seem to verify this stratigraphic division, and supports the proximal evidence of two closely spaced yet temporally separate eruptions. Tephra (BIW07-06) 8.84-8.87 m in Lake Biwa has volcanic glasses which share major and trace element compositions consistent with SG06-2535, SG06-2534 and SG06-2504, including the more variable incompatible trace element ratios than the older DSs tephra. This data would support this layers previousassignment to the DHg (Takemura et al., 2010) butit is possible that it represents a composite of the ash fall events associated with both HgA and HgP, which are recorded separately at Lake Suigetsu **(Fig., 7C-D)**. Importantly the SG06 stratigraphy confirms that the MsP flow deposits were not contemporaneously emplaced during the DHg activities, as proposed by Yamomoto (2017).

4.2.1 Pre-AT activity

Two CA tephra layers, SG06-4281 and SG06-4318 (silicic end-member only; **Fig. 8**), stratigraphically below the AT tephra and beyond the limit of varved and ^{14}C dated sediments in the Lake Suigetsu record, are unequivocally related to Daisen activity based on their major and trace element glass chemistry **(Fig. 4, 8; Sup. Fig.1)**. The Lake Suigetsu age-depth model provides ages of 59.6 ± 5.4 ka (95.4%) and 61.1 ± 5.8 (95.4%) for SG06-4281 and SG06-4318, respectively. SG06-4318 also has a basaltic glass component (Smith et al., 2013), which may represent a mafic injection triggering the eruption. Here we concentrate on the silicic end-member of SG06-4318, as we were unsuccessful in characterising the mafic glasses at a trace element level.

Major element data indicate both SG06-4281 and SG06-4318 silicic glasses lie on a clear fractionation/evolutionary trend (**Fig. 4**), which offers crucial insights into the evolution of the Daisen magmas. The more evolved SG06-4281 glasses (higher SiO_2, and lower CaO and FeOt contents) are enriched in many incompatible elements (e.g., Th, Rb, La, Ce; **Fig., 2F**), but more depleted in the middle and heavy REE (**Fig. 2F; Fig. 5C**) relative to SG06-4318. These REE elements are compatible in hornblende and biotite, which are abundant phases in the eruptive products of Daisen and Sambe (e.g., Machida and Arai, 2003), indicating depletions in the middle and heavy REE are in part driven by fractionation processes. The SG06-4318 glasses have similar Zr contents compared to those of the more evolved SG06-4281 glasses suggesting the melts are fractionating zircon (**Fig., 5A**). Interestingly, significant variations in Zr content are observed in the glasses of both Daisen and Sambe volcanoes with increasing evolution (e.g., increasing Th content; **Fig. 5A**). Both Zr and Y contents of the melts are being depleted through fractionation processes (**Fig. 5B**) and therefore lower Y/Th and Zr/Th ratios are the product of greater degrees of evolution. It is clear the melts erupted at Sambe are broadly more evolved than those erupted at Daisen as also demonstrated by their extension to higher SiO_2 and lower CaO and FeOt (**Fig. 4**).

East of Daisen, three prominent eruptive units reside between the AT and Aso-4 tephra layers and must be considered as proximal candidates of the SG06-4281 and SG06-4318 tephra layers. They are the Daisen Kurayoshi Pumice (DKP), the Sekigane Pumice (DSP) and the Namadake Pumice (DNP) (**Table 1**). These three poorly dated Plinian fall units are separated by palaeosols, and are incredibly weathered making characterisation of their volcanic glasses extremely challenging (e.g., Furusawa, 2008). The youngest of these three Plinian eruptions, the DKP, is the most widely traced through detailed mapping (e.g., Machida and Arai, 1979), with ash dispersed north-east towards the Pacific coast of Japan (**Fig**., **1**; Machida and Arai, 2003; Takemoto, 1991; Yamamoto, 2017).

Attempts were made to compare the Daisen derived SG06-4281 and SG06-4318 layers to the glass compositions from pumices collected from the *Daisen Lake* pre-AT type locality situated 15 km east of vent towards Kurayoshi City (**Supplementary material 1**). Unfortunately, the DKP, DSP and DNP units are heavily weathered at the site (Furusawa, 2008) making clear stratigraphic divisions extremely difficult to assess. We recovered some pumice fragments from a weathered deposit below the AT tephra but it was not immediately clear which stratigraphic unit they belong to. Owing to paucity of proximal juvenile glass data, we rely on the published plagioclase melt inclusion data from the deposits at *Daisen Lake* (Furusawa, 2008). Our pumice matrix glasses show similar levels of geochemical evolution to the melt inclusion data from the DSP and DNP eruptive units, but the matrix glasses are significantly less evolved than the DKP melt inclusion data (**Fig. 8**). Since melt inclusion data should be similar, or slightly less evolved than the host melt compositions, these matrix glasses must be from the DSP or DNP eruption units **(Fig. 8)**.

The glass compositions of the SG06-4281 tephra are most consistent with the DKP melt inclusion data (**Fig. 8**). Given that DKP ash fall is traced extensively north-east of Daisen, we compare the SG06-4281 glass data with two distal candidates of DKP ash fall. The first layer, TKN1080 (Nagahashi et al., 2007; Kimura et al., 2015), is recorded in the Takano Formation (**Fig. 1**), whilst a second layer is reported in a borehole 600 km north-east of Daisen in Naka-iwata, Aizu-bange town (Suzuki et al., 2016) (**Fig. 1**). SG06-4281 glasses show strong major and trace element agreement with the compositions of these distal ash layers, particularly the Nakai-wata borehole layer at 30.18m depth which was re-analysed here (**Table 4**). This glass data confirms that the SG06-4281 layer relates to this extremely widespread DKP Daisen ash dispersal extending north-east across Japan.

The underlying layer in Lake Suigetsu, SG06-4318, has felsic glasses that are instead geochemically similar to the less evolved matrix glasses of our sample, which is also chemically consistent with the melt inclusion data from the DSP and DNP eruption units. DNP can be excluded as the proximal candidate of SG06-4318 based on its distribution and chrono-stratigraphy. Isopach mapping sees DNP fall distribution extend towards the southern shores of Lake Biwa (Yamamoto, 2017), south of Lake Suigetsu. Furthermore, DNP is dated at ca. 80 ka (**Table 1**), and is considered closer in age to Aso-4 (87.5 ka) than the overlying DSP based on the relative thicknesses of intervening paleosols (Furusawa, 2008). The DSP eruption deposits are instead mapped eastward towards Lake Suigetsu (Yamamoto 2017, references therein). With DNP excluded, and SG06-4281 assigned to the DKP eruption unit, we tentatively suggest the SG06-4318 relates to the DSP eruption unit. The poor preservation of volcanic glass in these Daisen eruption deposits in the proximal areas makes it very difficult to make robust tephra correlations. Consequently, there is enormous benefit to using the chrono-stratigraphy and geochemistry of Daisen tephra layers

recorded in Lake Suigetsu when correlating and mapping these Pre-AT Daisen ash dispersals.

4.3 The other SG06 tephra layers displaying a SWJA signature

Three SG06 tephra layers considered to originate from the SWJA explosive activity remain more challenging to assign specifically to either Sambe or Daisen eruptions on the basis of the geochemical criteria outlined in Section 3. Two layers are situated stratigraphically between the AT and Aso-4. SG06-3974 lies just beyond the ^{14}C dated portion of the SG06 record, and has an age of 50.9 ± 0.4 ka (95.4%), whilst SG06-4141 (54.4 ± 1.6 ka [95.4%]) is stratigraphically above the SG06-4281/DKP and below SG06-4124/SUn (53.8 ± 1.0 ka [95.4%]) layers. The oldest tephra with a SWJA signature identified here in the Lake Suigetsu record (SG06-6457) is located below the Aso-4 tephra, and has an extrapolated age of 126.2 ± 8.2 ka (95.4%). Here we attempt to resolve their provenance using the geochemical information discussed above, and the developing proximal-distal chrono-stratigraphy.

All three tephra layers have major element glass compositions which are more evolved than currently characterised proximal Daisen glasses (higher SiO_2, lower CaO and FeOt), and consequently overlap with some deposits from Sambe (**Fig. 4**). Furthermore their glasses extend to K_2O contents higher than those observed in our existing proximal Daisen glass dataset (**Fig., 4A-B**). The increase in K_2O content observed in Sambe glasses coincides with a reduction in CaO and FeOt contents, which clearly reflects fractionation processes in the most evolved end-members (>76 wt.% SiO_2) (**Fig. 4**), which would not preclude similar processes affecting more evolved Daisen magmas. All three SG06 tephra layers show Zr/Th ratios that extend from values similar to those of Daisen glasses to lower values but these still remain higher than those observed in the silicic Sambe proximal glasses (**Fig. 4H**), suggesting that they are more likely to derive from Daisen volcano than Sambe.

If we consider the known eruptive activity of Daisen and Sambe (**Table 1**), no eruptive units at Sambe are chrono-stratigraphically consistent with SG06-3974 that is dated at ca. 50 ka. At Daisen however, the Kamagaoka fall (Machida and Arai, 2003) and the loosely associated Makibara flow (Yamamoto, 2017) are reported between the AT and DKP tephra deposits, though the former is possibly placed stratigraphically above the Sambe Ikeda (SI; Machida and Arai, 2003), which is inconsistent with the position of SG06-3974 below the believed SI in the Lake Suigetsu stratigraphy. Proximal stratigraphic uncertainties mean that it is difficult to assess the relevance of the Makibara pyroclastic flows to this SG06 tephra layer. The precise proximal link to a proximal unit at Daisen requires further investigations.

SG06-4141 is one of the thickest tephra units in the SG06 record to show a SWJA type trace element signature (Fig. 2B; **Table 2**). It is located stratigraphically just below the SUn (SG06-4124) and above DKP (SG06-4281) in the SG06 record. There are no prominent proximal deposits documented in outcrops around Sambe at this time, and it is unlikely that an eruption responsible for a 1.3 cm thick layer in Lake Suigetsu, 300 km away, is from an eruption not recorded in the Sambe volcanic stratigraphy (**Table 1**). Geochemically, levels of incompatible trace element enrichment in the SG06-4141 glasses are significantly higher than those observed in the older activities of Sambe volcano (Cycles I and II) (**Fig. 5**; SOd, SUn, SK), further evidence to preclude a source attribution.

Interestingly, SG06-4141 has a major element glass chemistry which is consistent with the SAN1 tephra layer reported from numerous Sea of Japan marine cores to the north-east of Daisen (**Fig., 8B; Ikehara et al., 2004; 2016).** Here we present new, more comparable glass data from two reported SAN1 layers in Sea of Japan cores GH89-2-25 and GH89-2-27 (Fig. 1; Ikehara et al., 2004). These glass data reinforce the geochemical agreement between this prominent marine layer and the SG06-4141 tephra (**Fig., 8A-B).** Ikehara et al., (2004) previously suggested that the SAN1 tephra, given its chemical composition and layer thickness, derived from Daisen volcano. These authors also suggest that owing to its position in records with an oxygen isotope stratigraphy it occurred at 53-55 ka and that it may relate to the DKP eruption. The SG06 tephrostratigraphy clearly indicates that the SG06-4141/SAN1 tephra is a chrono-stratigraphically distinct event to that associated with DKP (SG06-4281) activity at Daisen volcano. At Daisen volcano, above the DKP and below the AT tephra, no thick, prominent deposit is found in the same chrono-stratigraphic position as the SG06-4141/SAN1 layer. Therefore, we must consider the possibility that the SG06-4141/SAN1 tephra derives from a large eruption of another volcano with a SWJA type signature. Japanese tephra database (e.g., Machida and Arai, 2003) of explosive volcanism occurring on south-west Honshu do not record any alternative large magnitude events in the appropriate stratigraphic position. However, Kuju volcano, located in the Hohi Volcanic Zone (HVZ; Fig. 1), erupted the thick Handa pyroclastic flow deposits (Kj-Hd) at ca. 53.5 ka (Okuno et al., 2017). The age and major element compositions (Supplementary information) of Kj-Hd are consistent with those of SG06-4141/SAN1 (54.4 ± 1.6 ka) allowing us to suggest a correlation (Fig. 2A-B; Fig. 8). The HVZ (Fig. 1) is situated at the junction between the SWJA and the Ryukyu-Kyushu Arc (Kamata, 1998; Fig. 1) and according to Shibata et al. (2014) Kuju deposits have shown 'adakitic' signatures, that are characterised by low-Y/HREE contents, consistent with the SWJA volcanism.

The deepest SG06 tephra layer from the SWJA is located below Aso-4, SG06-6457. The SG06 age-depth model yields an age of ~126 ka for this tephra, which predates the onset of known activity at Sambe volcano (**Table 1**). Known Daisen eruptions below the Aso-4 tephra are the Plinian Hiruzenbara (DHP) and Matsue (DMP). The preferred age of DMP (**Table 1**) is entirely consistent with SG06-6457, but this tephra is predominantly thought to be dispersed west of Daisen away from Lake Suigetsu (Machida and Arai, 2003; Yamamoto, 2017). The age of the stratigraphically younger DHP proximal unit is not well constrained, but this tephra is dispersed to the east of Daisen (Machida and Arai, 2003). Determining the source deposits of this distal tephra demands further investigations of both near source candidates, assuming well preserved deposits suitable for chemical characterisation can be identified.

4.4 An Integrated proximal-distal eruption stratigraphy

The Lake Suigetsu sedimentary archive presents a detailed record of explosive eruptions at Sambe and Daisen volcanoes along the SWJA (**Fig. 3**). Through combining the wealth of geochemical, stratigraphical and chronological information preserved in this distal sedimentary record with that from the proximal volcanic setting we have generated an integrated, more detailed, proximal-distal event stratigraphy (**Fig. 9**). In the following sections we exploit this new volcanological information to elucidate a more precise and reliable eruptive history for the Sambe and Daisen stratovolcanoes.

The integrated proximal-distal record reveals that of the nine Daisen eruptions observed in the lake sediments at least six tephra layers can be related to fallout from Vulcanian to Plinian activities, whilst a further two are linked to pyroclastic flows probably associated with dome collapses (**Fig. 9**). Of the five Sambe eruptions recorded as tephra layers in the SG06 record, two relate to Plinian fall activities and three to the emplacement of pyroclastic flows, with at least one attributed to a dome collapse event (Th-pd). There are some notable absences from the SG06 tephra record given their thickness in proximal settings, and this is likely to reflect unfavourable dispersal axis. For instance the sub-Plinian/Plinian fall associated with Daisen Kusadanihara (DKs), which is exposed to the north of the Daisen summit (Domitsu et al., 2002; Yamamoto, 2017), and the Daisen Namatake (DNP) Plinian eruption, which is dispersed E/SE towards the southern shores of Lake Biwa (Yamamoto, et al., 2017) are both absent from the Lake Suigetsu stratigraphy. The Sambe Plinian Kisuki (SK) eruption (**Table 1**) has a strong north-easterly dispersal mapped just to the north of Lake Suigetsu (Machida and Arai, 2003). The absence of visible tephra layers associated with large magnitude eruptions at Daisen and Sambe does not preclude their future identification as non-visible cryptotephra horizons in the Lake Suigetsu record. Indeed in European distal tephrostratigraphic investigations, the mapped distribution of ash fall from many large eruptions have been greatly extended through the identification of cryptotephra layers (e.g., Blockley et al., 2007; Lowe et al., 2015; Albert et al., 2015). Ongoing cryptotephra investigations through the Lake Suigetsu sediments will resolve many additional tephra fall layers, and dramatically extend known ash dispersals of Japanese eruptions (e.g., McLean et al., 2018).

Erroneous proximal-distal tephra correlations revealed here highlight the importance of glass chemistry to establish robust correlations, particularly during complex periods of explosive volcanism, when multiple eruptive units are emplaced in close succession. For instance the Sambe Ukinuno pumice *(*Suk*/*U2) eruption at the end of the last glacial period was thought to be the proximal equivalent of the widespread distal ash layer the *Sakate* tephra traced across central Japan (Machida and Arai, 2003; Katoh et al., 2007) but new geochemical data reveal that SG06-1965/Sakate tephra are instead distal ash dispersed during the Midorigaoka pyroclastic flow (Md-fl). As such, the ash from this sub-Plinian eruption is not preserved in the SG06 record and therefore it is not clear that it was as widely dispersed as previously proposed (Machida and Arai, 2003; Katoh et al., 2007).

4.4.1 High-precision SG06 chronological constraints and implications for eruptive frequency

The high-precision chronology of the Lake Suigetsu sedimentary archive allows us to place new age constraints on the timing of explosive eruptions from Sambe and Daisen volcanoes (**Table 2; Fig. 9)**, along with the ability to differentially date eruptions (**Table 5**). For Daisen and Sambe SG06 tephra layers preserved in the ^{14}C/varved portion of the record we can provide very precise eruption ages, significantly improving upon previous ^{14}C dates of charcoal from within source deposits, for instance the Sambe Holocene eruptions Taihezan (Th-pd) and Shigaku (S2-fl) (**Fig. Sup2A).** Owing to the inherent difficulties of directly dating CA tephra deposits outside the radiocarbon timeframe (>50 ka), many of these older Daisen and Sambe proximal tephra layers are poorly constrained in age (**Table 1**). Consequently, even beyond the precisely dated portion of the SG06 record, the age-depth model still provides the most reliable eruption ages for the tephra preserved in the sequence. For instance, the age-depth model provides an age of 59.6 ± 5.4 ka (95.4%) for SG06-4281, the

672 Kurayoshi pumice eruption unit (DKP) that is the most widespread Late Quaternary ash
673 dispersal from Daisen volcano and is found over 600 km NE of the volcano to Naka-iwata,
674 Aizu-bange town (**Fig. 1**). This widespread tephrostratigraphic marker is particularly
675 important for Quaternary studies in central Japan focusing on constraining events around the
676 marine isotope stage 3/4 transition.

677 Crucially the SG06 sedimentary record captures two intervals of significant unrest at Daisen
678 volcano:

679 **(1) 61.1-50.4 ka (3 eruptions/ash dispersals)**

680 Three Daisen derived layers are recognised beneath the AT tephra and these were erupted
681 in a period that spanned approximately 10 ka and this includes the widespread DKP ash
682 dispersal (SG06-4281). Importantly from a hazard point-of-view, SG06-4281 (DKP) and
683 SG06-4318 (DSP) Plinian eruptions of Daisen are separated by ~1,500 years according to
684 the SG06 age-depth model.

685 **(2) 29,935-28,370 IntCal13 yrs BP (5 eruptions/ash dispersals)**

686 Explosive activity resumes at Daisen after ~20 ka of quiescence, 246 years after the caldera
687 forming AT eruption in southern Kyushu (**Table 5; Supplementary Fig. 3**), with the
688 emplacement of the Sasaganaru or Shitano-hoki pyroclastic flow deposits (SG06-2602), that
689 are related to the collapse of the Karausgasen lava dome (Kimura, et al., 2005; Yamomoto,
690 2017). The SG06 sediment record confirms an eruption hiatus, between the Sasaganaru
691 pyroclastic flows and the upper Odori ash fall (OdA), which has also been suggested by
692 Kimura et al., (2005), where they identified a thin humic palaeosol between the units close to
693 the volcano. The SG06 IntCal13 age-depth model suggests a median differential age of 6
694 years separating these two explosive eruptions (**Table 5; Supplementary Fig. 3**).

695 The SG06 archive then indicates there was a short period of quiescence or less explosive
696 activity, lasting between 830-1036 IntCal13 years (**Table 5**), between the OdA fall (SG06-
697 2601) and the Higashi-daisen, HgA/SG06-2535 eruptions. The two closely spaced, Higashi-
698 daisen eruptions, SG06-2535/HgA and SG06-2534/HgP, have a median differential age of 5
699 years (**Table 5; Supplementary Fig. 3**). Then there is another 363-516 IntCal13 years
700 (95.4%) between the sub-Plinian/Plinian eruption which produced the HgP fall deposits and
701 the emplacement of the Mazumizahara (MsP) pyroclastic flows (SG06-2504).

702 Tephra fall associated with the more recent Daisen eruptions are not recorded in SG06 as
703 visible layers (**Fig. 9**). Tephra from the sub-Plinian fall deposits of the Daisen Kusatanihara
704 (DKs) pumice (**Table 1**) are reported north-east of Daisen and are found in the Sea of Japan
705 marine sediments (Domitsu et al., 2002) and also in those of Ichi-no-Megata in north-
706 western Honshu (Okuno et al., 2011). New trace element glass chemistry (**Table 4**) from the
707 tephra IMG06-16.35m in Ichi-no-Megata unequivocally supports this correlation to explosive
708 volcanism at Daisen as the glasses have low Y and HREE contents (**Fig. 5B; Table 4**).
709 Major element glass compositions reinforce that IMG06-16.35m is similar in composition to
710 proximal DKs pumices characterised here (**Supplementary material 1**) and in Domitsu et
711 al., (2002; **Fig. 7**). The ^{14}C age-depth model of Ichi-no-Megata (Okuno et al., 2011) provides
712 an age of 22,330-22,790 IntCal13 yrs BP (95.4%) for this eruption. The Ichi-no-Megata distal
713 age for DKs eruption is younger than the proximal age derived for the MsP and is older than
714 the age of the Amidagawa (AmP)/Misen (MiF) flows (**Table 1; Supplementary Figure 2C**)

dated at between 20,637-21,015 IntCal13 yrs BP (Yamamoto, 2017). These chronological constraints suggest a period of quiescence of ~5,500 years between the MsP and the DKs sub-Plinian/Plinian eruption (**Supplementary Fig. 2C**), which was closely followed by the most recent Daisen activity of the Amidagawa/Misen flows. The full chronology of the Post-AT eruptions at Daisen volcano is summarised in **Supplementary Figure 2**. The new chronological insights into the tempo of pre-historic eruptions at Daisen are essential to future hazard assessments of the volcano. The volcano clearly experiences pulses of intense activity that are separated by long repose intervals of thousands of years. Therefore, the renewal of activity following the current period of quiescence is unlikely to be characterised by a single eruption and associated ash dispersal.

4.4.2 Implications for eruptive magnitude and volume estimates

The integrated Daisen and Sambe proximal and distal (SG06) event stratigraphy confirms stratigraphic and temporal separation of eruptive units previously considered as single volcanic events. This has clearly implications for the accuracy of magnitude and volume estimates for eruptions from Daisen in particular. For instance, Daisen Sasaganaru (DSs) is classified as a VEI 5 eruption (Machida and Arai, 2003; Hayakawa, 2010), yet the high-resolution sedimentation at Lake Suigetsu means that the SG06 record indicates there are two large ash dispersals associated with the DSs eruption deposits, with a temporal gap between the Sasaganaru flows (SaF) and Odori Ash (OdA) fall phases. Previous grouping of these proximal units has led to an underestimation of eruptive frequency and an overestimation of the magnitude and volume. Indeed, Yamamoto (2017) combined volumes estimates of the Sasaganaru flows (1.0 km^3 DRE), the Odori fall (0.44 km^3 DRE) and the Karasugasen lava flow (0.07 km^3 DRE) into a total eruption volume estimate at 1.5 km^3 DRE. However, these estimates should be considered separately as they do not represent a single volcanic event in time **(Table 2; Table 5).** Furthermore, the Daisen eruption chronology elucidated by the SG06 sediment record also reveals that the Higashi-daisen (DHg) fall events and the Masumizuhara (MsP) flows were temporally separate events (**Table 5; Supplementary Figure 2C**), inconsistent with the interpretation of Yamamoto (2017) and consequently their eruption volumes should also be considered separately.

Interestingly, Machida and Arai (2003) report the DSs deposits as representing a larger magnitude eruption than the overlying Higashi-daisen (DHg) tephra. Yet the Lake Suigetsu correlative of the Higashi-daisen pumice fall (HgP), SG06-2534 (0.6 cm), is thicker than the distal equivalent of the Sasaganaru flow layer, SG06-2602 (0.4 cm) (**Table 2**). Whilst this greater thickness might be merely a function of a preferential dispersal axis it may also suggest the Higashi-daisen eruptive magnitude has been previously underestimated. In the Lake Biwa core BIW07-06 the Daisen derived layer at 8.84-8.87 m (3 cm) related to Higashi-daisen is considerably thicker than the underlying two closely spaced Daisen layers 9.380-9.385m and 9.370-9.375m, which are geochemically linked to the Sasaganaru flow (0.5 cm) and Odori fall (0.5 cm) respectively (**Fig. 9**). This might provide further support for the interpretation that Higashi-daisen pumice fall eruption represents the single largest eruption of Daisen volcano in the post-AT interval, and that its eruption volume has been underestimated.

In the SG06 stratigraphic record, below the AT, the closely spaced Daisen tephra layers between 61.1-50.4 ka testify to a period of unrest characterised by closely spaced large explosive eruptions of the volcano, including the DKP/SG06-4281 and DSP/SG06-4318

(**Fig., 9**). Whilst there is little doubt that SG06-4281 relates to the dramatically widespread ash dispersal north-east across Japan, the 11 km^3 DRE estimated volume of the DKP eruption (Yamamoto, 2017) is greatly constrained by medial and distal occurrences of tephra fall (Machida and Arai, 2003). Given the close succession of Daisen layers in SG06, and that the chronology of the host records are often poorly constrained in this time interval, we recommend that all distal occurrences of tephra layers thought to be DKP distal ash are geochemically analysed and these data are compared to the Daisen layers in the SG06 record. This is crucial for robust tephra correlations and using these tephra as absolute age markers in distal records. Furthermore it will provide critical information required to re-assess the ash dispersals and volume estimates associated with the individual Daisen eruptions.

As discussed earlier in relation to Sambe volcano, the re-assessment of the proximal equivalent of the distal Sakate/SG06-1965 tephra that erupted at the end of the last glacial period, has implications for volume/magnitude estimates of the Ukinuno sub-Plinian pumice fall eruption which is currently considered at least a VEI 5 (Machida and Arai, 2003; Hayakawa, 2010). A proximal-distal miscorrelation means that this widespread ash dispersal across much of central Japan (*Sakate* tephra=SG06-1965) is not related to the Unkinuno sub-Plinian pumice fall (U2) event, and instead is linked to the Midorigaoka pyroclastic flow (Md-fl) deposits. Consequently, the current magnitude estimates for Ukinuno pumice fall eruption are likely to be overestimated.

4.4.3 SWJA magma genesis, chemical evolution and repeated glass chemistries

Our extensive glass dataset for the Daisen and Sambe magmas displays steep mantle normalised trace element profiles with depletions in the HREE and yttrium (**Fig. 2**). These trends have been observed before, with it being suggested that the are due to the stabilization of garnet at a high pressure (>2 GPa) during formation of the primary SWJA dacite magmas, with slab melting of the subducting hot-young Shikoku Basin plate responsible for extremely low middle to heavy REE concentrations (Morris, 1995; Feineman et al., 2013; Kimura et al., 2014; 2015). Our new glass data also show the response of trace elements to fractionation processes, which can be observed by comparing the SG06-4318 and SG06-4281 tephra layers (**Fig. 8**). Both these Daisen tephra lie on clear major element fractionation trends and there are greater depletions in the Y/REE contents observed in the more silicic melt compositions (SG06-4281), indicating the source feature is at the very least being overprinted by high-level magma chamber fractionation processes (e.g., hornblende/biotite fractionation (**Fig. 2; 5C**) as suggested in previous studies (Kimura et al., 2014; 2015). Sambe glass compositions reveal magmas have become enriched in incompatible trace elements through time. Despite all erupted magmas being highly silicic (>70 wt.% SiO_2), older magmas associated with eruptive cycle I (Kisuki) and cycle II (Unnan and Oda) are characterised by significantly lower levels of enrichment of certain incompatible trace elements (e.g., Th and LREE), whilst others are more enriched (e.g., U) relative to the younger activities of cycles IV-VII. Interestingly, Sambe tephra SG06-3668/Ikeda (cycle III) glasses provide evidence for the arrival of melts more enriched in incompatible trace element concentrations, and only through the glass chemistry of the distal layers (SG06-3668 and BIWA07-06 16.02-16.04m) analysed here, can we observe interaction between the new melts and remnants associated with the older cycles (**Fig. 6**). Finally, these geochemical data reveal that both Daisen and Sambe repeatedly erupt volcanic glasses with overlapping compositions (**Fig. 6-8**). Consequently, correlating proximal-distal tephra relies on good stratigraphic and chronological control, and is best

achieved in sedimentary archives which preserve comprehensive catalogues of ash fall events like Lake Suigetsu.

5. Conclusions

This study highlights the advantages of integrating information from the proximal volcanic stratigraphies and detailed distal sedimentary records with high-resolution chronologies. The annually laminated (varved) and intensely dated (^{14}C) lacustrine sediments of Lake Suigetsu, Honshu Island, Japan, are ideally placed to apply chronological constraints on the timing and frequency of volcanism at Sambe and Daisen stratovolcanoes along the SWJA. Trace element volcanic glass chemistry were used to verify the visible ash (tephra) layers preserved in the SG06 sediment sequence that related to past explosive eruptions of these two volcanoes. The integrated proximal-distal event stratigraphy (**Fig. 9**) confirms that Lake Suigetsu preserves ash fall from nine Daisen and five Sambe explosive eruptions, which owing to the unrivalled chronology of this archive are more precisely dated than ever before. The Lake Suigetsu sediments capture two periods of significant unrest at Daisen that are characterised by closely spaced and widespread ash dispersals. The first period begins at ~ 61.9 ka with three explosive eruptions over ~ 10 ka. The Lake Suigetsu sediments reveal two of these eruptions were separated by as little as 1,500 years. One of these two layers (SG06-4281) relates to the most widespread Late Quaternary Daisen ash dispersal linked to the DKP eruption which is traced over 600 km from source, yet this eruption is not responsible for the SAN1 marine tephra layer (Sea of Japan). Following a period of quiescence at Daisen volcano, the Lake Suigetsu record catalogues a succession of five eruptions and widespread ash dispersal from Daisen beginning at 29,837 ± 96 IntCal13 yrs BP. High-precision differential dating using the SG06 IntCal13 age-depth model reveals these events were separated by 6, 932, 5 and 438 IntCal13 years. The integrated proximal-distal eruption event stratigraphy, which provides new high-precision stratigraphic and chronological constraints, offers unique insights into the frequency of past explosive eruptions and widespread ash dispersals. The SG06 high-resolution sedimentary record has enabled the verification of multiple closely spaced eruptions at Daisen volcano which have important implications for existing magnitude estimates and hazard assessments.

Acknowledgements:

The authors would like to thank: Dr. Daisuke Endo, Shimane Nature Museum of Mt. Sambe, for providing samples catalogued in the Database of research materials of Sambe Volcano collected by Seiji Matsui (2010) and Database of research materials of Sambe Volcano collected by Seiji Matsui and Takashi Fukuoka (2014); and Prof. Hiroshi Machida for providing the SAN1 marine tephra samples from the Sea of Japan. PGA was supported by a Leverhulme Trust Early Career Fellowship (ECF-2014-438), and TN acknowledges support from KAKENHI Grant-in-Aid for Scientific Research (16K13894). The Lake Suigetsu SG14 core (formally 'Fukui-SG14') was recovered and provided for research by Fukui prefecture. The authors would also like to thank the anonymous reviewer for their positive feedback on a earlier version of the manuscript.

References:

Albert, P.G., Tomlinson, E.L., Lane, C.S., Wulf., S., Smith, V.C., Coltelli, M., Keller, J., Lo Castro, D., Manning, C.J., Muller, W., Menzies, M.A., 2013. Late glacial explosive activity on

849 Mount Etna: implications for proximal-distal tephra correlations and the synchronisation of
850 Mediterranean archives. Journal of Volcanology and Geothermal Research, 265, 9-26.

851 Albert, P.G., Hardiman, M., Keller, J., Tomlinson, E.L., Bourne, A.J., Smith, V.C., Wulf, S.,
852 Zanchetta, G., Sulpizio, R., Müller, U.C., Pross, J., Ottolini, L., Matthews, I.P., Blockley, S.P.,
853 Menzies, M.A., 2015. Revisiting the Y-3 tephrostratigraphic marker: a new diagnostic glass
854 geochemistry, age estimate, and details on its climatostratigraphic context. Quaternary
855 Science Reviews 118, 105-122.

856 Blockley, S.P.E., Lane, C.S., Lotter, A.F., Pollard, A.M., 2007. Evidence for the presence of
857 the Vedde Ash in Central Europe. Quaternary Science Reviews 26, 25-28, 3030-3036.

858 Bourne A.J., Albert, P.G., Matthews, I.P., Wulf, S., Lowe, J.J., Asioli, A., Blockley, S.P.E.,
859 Trincardi, F., 2015. Tephrochronology of core PRAD1-2 from the Adriatic Sea: insights into
860 Italian explosive volcanism for the period 200-80ka. Quaternary Science Reviews, 116, 28-
861 43.

862 Bronk Ramsey, C., 2008. Depostional models for chronological records. Quaternary Science
863 Reviews, 17, 1-2, 42-60.

864 Bronk Ramsey, C., Staff, R.A., Bryant, C.L., Brock, F., Kitagawa, H., van der Plicht, J.,
865 Schlolaut, G., Marshall, M.H., Brauer, A., Lamb, H.F., Payne, R.L., Tarasov, P.E.,
866 Haraguchi, T., Gotanda, K., Yonenobu, H., Yokoyama, Y., Tada, R., Nakagawa, T., 2012. A
867 complete terrestrial radiocarbon record for 11.25 to 52.8 kyr BP. Science 338, 370e374.
868 http://dx.doi.org/10.1126/science.1226660.

869 de Fontaine, C. S., Kaufman, D. S., Anderson, R. S., Werner, A., Waythomas, C, F., Brown,
870 T.A., 2007. Late Quaternary distal-fall deposits in lacustrine sediments, Kenai Peninsula,
871 Alaska. Quaternary Research 68, 64-78.

872 Domistu, H., Shiihara, M., Torii, M., Tsukawaki, S. and Oda, M., 2002. Tephrostratigraphy of
873 the piston cored sediment KT96-17 P-2 in the southern Japan Sea—the eruption age of
874 Daisen-Kusadanihara Pumice (KsP)—. Journal of the Geological Society of Japan, 108:
875 545-556. (In Japanese with English abstract)

876 Feineman, M., Moriguti, T., Yokoyama, T., Terui, S. and Nakamura, E., 2013. Sediment-
877 enriched adakitic magmas from the Daisen volcanic field, Southwest Japan. Geochem.
878 Geophys. Geosysts., 14 (8).

879 Fukuoka, T. 2005. ^{14}C ages of the Stage IV pyroclastic deposits at Sanbe Volcano. Bulletin
880 of the Shimane Nature Museum of Mt. Sanbe (Sahimel), 3: 61-64. (In Japanese with English
881 abstract)

882 Fukuoka, T. and Matsui, S., 2002. Stratigraphy of pyroclastic deposits post-dating the AT
883 tephra, Sambe Volcano. Earth Science (Chikyu Kagaku), 56: 105-122. (In Japanese with
884 English abstract)

885 Furusawa, A., 2008. Characterizing tephra by major-element analysis of glass inclusions in
886 the plagioclase phenocrysts: Preliminary results from the DKP tephra of Daisen volcano,
887 Japan. Jour. Geol. Soc., Japan, 114, 12, 618-631.

888 Giaccio, B., Niespolo, E., Pereira, A., Nomade, S., Renne, P.E., Albert, P.G., Arienzo, I.,
889 Regattieri, E., Wagner, B., Zanchetta, G., Gaeta, M., Galli, P., Mannella, G., Peronace., E.,
890 Sottili, G., Florindo, F., Leicher, N., Marra, F., Tomlinson, E.L., 2017. First integrated
891 tephrochronological record for the last ~190 kyr from the Fucino Quaternary lacustrine
892 succession, central Italy. Quaternary Science Reviews 158, 211-234.

893 Hayakawa, Y., 2010. Hayakawa's 2000-year eruption database and one million year tephra
894 database. http://www.hayakawayukio.jp/database. Accessed regularly.

895 Ikehara K, Kikkawa K, Chun JH. Origin and correlation of three tephras that erupted during
896 oxygen isotope stage 3 found in cores from the Yamato Basin, central Japan Sea. The Quat
897 Res (Daiyonki-kenkyu). 2004; 43: 201–12 (In Japanese with English abstract).

898 Ikehara, K., 2015. Marine tephra in the Japan Sea sediments as a tool for paleoceanography
899 and paleoclimatology. Progress in Earth and Planetary Science 2: 36.

900 Jochum, K.P., Stoll, B., Herwig, K., Willbold, M., Hofmann, A.W., Amini, M., Aarburg, S.,
901 Abouchami, W., Hellebrand, E., Mocek, B., Raczek, I., Stracke, A., Alard, O., Bouman, C.,
902 Becker, S., Dücking, M., Brätz, H., Klemd, R., de Bruin, D., Canil, D., Cornell, D., de Hoog,
903 C., Dalpé, C., Danyushevsky, L., Eisenhauer, A., Gao, Y., Snow, J.E., Groschopf, N.,
904 Günther, D., Latkoczy, C., Guillong, M., Hauri, E., Höfer, H.E., Lahaye, Y., Horz, K., Jacob,
905 D.E., Kasemann, S.A., Kent, A.J.R., Ludwig, T., Zack, T., Mason, P.R.D., Meixner, A.,
906 Rosner, M., Misawa, K., Nash, B.P., Pfänder, J., Premo, W.R., Sun, W.D., Tiepolo, M.,
907 Vannucci, R., Vennemann, T., Wayne, D., Woodhead, J.D., 2006. MPI-DING reference
908 glasses for in situ microanalysis: 581 New reference values for element concentrations and
909 isotope ratios. Geochemistry Geophysics Geosystems 7(2).

910 Kamata, H., 1998. Quaternary volcanic front at the junction of the South-west Japan Arc and
911 the Ryukyu Arc. Journal of Asian Earth Sciences 16 (1), 67-75.

912 Katoh, S., Handa, K., Hyodo, M., Sato, H., Nakaura, T., Yamashita, T., Danahara, T., 2007.
913 Estimation of eruptive ages of the Late Pleostocene tephra layers derived from Daisen and
914 Sambe Volcanoes based on AMS- 14C dating of moor sediments at Ohnuma Moor in the
915 Chugoku Mountains, Western Japan. Nature and Human Activities, 11, 29-50.

916 Kigoshi, T., Kumon, F., Hayashi, R., Kuriyama, M., Yamada, K., Takemura, K., 2014.
917 Climate changes for the past 52 ka clarified by total organic carbon concentrations and
918 pollen composition in Lake Biwa, Japan. Quaternary International 333, 2-12.

919 Kitagawa, H., Fukuzawa, H., Nakamura, T., Okamura, M., Takemura, K., Hayashida, A.,
920 Yasuda, Y., 1995. AMS ^{14}C dating of varved sediments from lake Suigetsu, Central Japan
921 and atmospheric 14C change during the Lake Pleistocene. Radiocarbon 37, 371-378.

922 Kitagawa, H. and van der Plicht, J. 1998a. Atmospheric radiocarbon calibration to 45,000 yr
923 B.P.: Late Glacial fluctuations and cosmogenic Isotope production, Science, 279: 1187-1190

924 Kitagawa, H. and van der Plicht, J. 1998b. A 40,000-year varve chronology from Lake
925 Suigetsu, Japan; extending the (super 14) C calibration curve, Radiocarbon, 40: 505-515

926 Kitagawa, H. and van der Plicht, J. 2000. Atmospheric radiocarbon calibration beyond
927 11,900 cal Bp from Lake Suigetsu laminated sediments, Radiocarbon, 42: 370-381

928 Kimura, J.-I., Tateno, M., Osaka, I., 2005. Geology and geochemistry of Karasugasen lava
929 dome, Daisen-Hiruzen Volcano Group, southwest Japan. The Island Arc 14, 115-136.

930 Kimura, J.-I., Gill, J.B., Kunikiyo, T., Osaka, I., Shimoshiori, Y., Katakuse, M., kakubuchi, S.,
931 Nagao, T., Furuyama, K., Kamei, A., Kawabata, H., Nakakima, J., van Keken, P.E., Stern,
932 R.J., 2014. Diverse magmatic effects of subducting a hot slab in SW Japan: Results from
933 forward modeling. Geochem. Geophys. Geosysts., 15, 691-739.

934 Kimura, J-I., Nagahashi, Y., Satoguchi, Y., Chang, Q., 2015. Origins of felsic magmas in
935 Japanese subduction zone: Geochemical characterizations of tephras from caldera-forming
936 eruptions <5Ma. Geochem. Geophys. Geosysts., 16, 2147-2174,
937 doi:10.1002/2015GC005854.

938 Kiyosugi, K., Connor, C., Sparks, R.S.J., Crosweller, H.S., Brown, S.K., Siebert, L., Wang,
939 T., Takarada, S., 2015. How many explosive eruptions are missing from the geological
940 record? Analysis of the quaternary record of large magnitude explosive eruptions in Japan.
941 Journal of applied Volcanology 4:17.

942 Lowe, J.J., Bronk Ramsey, C., Housley, R. A., Lane, C.S., Tomlinson, E.L., RESET Team,
943 RESET Associates 2015. The RESET project: constructing a European tephra lattice for
944 refined synchronisation of environmental and archaeological events during the last c. 100 ka.
945 Quaternary Science Reviews, 118, 1-17.

946 Machida, H., Arai, F., 1979. Daisen Kurayoshi Pumice: Stratigraphy, Chronology,
947 Distribution and implication to Late Pleistocene Events in Central Japan. Journal of
948 Geography, 88, 5, 313-330.

949 Machida, H. and Arai, F., 2003. Atlas of tephra in Japan and its surrounding area, 2nd edition.
950 University of Tokyo Press, Tokyo, 336p. (In Japanese, title translated)

951 Maruyama, S., Hattori, K., Hirata, T., Danahara, T., 2016. A proposed methodology for
952 analyses of wide-ranged elements in volcanic glass shards in widespread Quaternary
953 tephras. Quaternary International 397, 267-280.

954 Marshall, M., Schlolaut, G.,Nakagawa, T.,Lamb, H., Brauer, A., Staff, R., Bronk Ramsey, C.,
955 Tarasov, P., Gotanda, K., Haraguchi, T., Yokoyama, Y., Yonenobu, H., Tada, R., Suigetsu
956 2006 Project Members, 2012. Anovel approach to varve counting using mXRF and X-
957 radiography in combination with thin-section microscopy, applied to the Late Glacial
958 chronology from Lake Suigetsu, Japan. Quaternary Geochronology 13, 70-80.

959 McLean, D., Albert, P.G., Nakagawa, T., Suzuki, T., Staff, R. A., Yamada, K., Kitaba, I.,
960 Suigetsu 2006 Project Members; Smith, V.C., 2018. Integrating the Holocene
961 tephrostratigraphy for East Asia using a high-resolution cryptotephra study from Lake
962 Suigetsu (SG14 core), central Japan. Quaternary Science Reviews 183, 36-53.

963 McLean, D., Albert, P.G., Nakagawa, T., Staff, R., Suzuki, T., Suigetsu 2006 Project
964 Members; Smith, V.C., 2016. Identification of the Changbaishan 'Millennium' (B-Tm) eruption
965 in the Lake Suigetsu (SG06) sedimentary archive, Japan: Synchronisation of hemispheric-
966 wide palaeoclimate archives. Quaternary Science Reviews 150, 301-307.

967 Morris, P.A., 1995. Slab melting as an explanation of Quaternary volcanism and aseimicity in
968 southwest Japan. Geology, 25 (5), 395-398.

969 Nagahashi, Y., Sato, T., Takeshita, Y., Tawara, T., Kumon., 2007. Stratigraphy and
970 Chronology of Widespread Tephra Beds Intercalated in TKN-2004 Core sediment Obtained
971 from the Takano Formation, Central Japan. The Quaternary Research 46, 305-325.

972 Nakagawa, T., Gotanda, K., Haraguchi, T., Danhara, T., Yonenobu, H., Brauer, A.,
973 Yokoyama, Y., Tada, R., Takemura, K., Staff, R.A., Payne, R., Bronk Ramsey, C., Bryant,
974 C., Brock, F., Schlolaut, G., Marshall, M., Tarasov, P., Lamb, H., Suigetsu 2006 Project
975 Members, 2012. SG06, a fully continuous and varved sediment core from Lake Suigetsu,
976 Japan: stratigraphy and potential for improving the radiocarbon calibration model and
977 understanding of late quaternary climate changes. Quaternary Science Reviews 36,
978 164e176. http://dx.doi.org/10.1016/j.quascirev.2010.12.013.

979 Okada, S. and Ishiga, S., 2000. Tephras from Daisen Volcano. In Sawada, Y. and Nomura,
980 N. (ed.), Field Excursion Guidebook of the 107th Annual Meeting of the Geological Society of
981 Japan, Matsue, 81-90. (In Japanese)

982 Okuno, M., Nagaoka, S., Saito-Kokuba, Y., Nakamura, T., Kobayashi, T., 2017. AMS
983 radiocarbon dates of pyroclastic-flow deposits on the southern slope of the Kuju volcanic
984 group, Kyushu, Japan. Radiocarbon 59, 483-488.

985 Reimer, P.J., Bard, E., Bayliss, A., Beck, J.W., Blackwell, P.G., Ramsey, C.B., Buck, C.E.,
986 Cheng, H., Edwards, R.L., Friedrich, M. and Grootes, P.M. 2013. IntCal13 and Marine13
987 radiocarbon age calibration curves 0–50,000 years cal BP. Radiocarbon, 55: 1869-1887.

988 Schlolaut, G., Marshall, M., Brauer, A., Nakagawa, T., Lamb, H., Staff, R., Bronk Ramsey,
989 C., Bryant, C., Brock, F., Kossler, A., Tarasov, P., Yokoyama, Y., Tada, R., Haraguchi, T.,
990 Suigetsu 2006 Project Members, 2012. An automated method for varve interpolation and its
991 application to the Late Glacial chronology from Lake Suigetsu, Japan. Quaternary
992 Geochronology 13, 52e69. http://dx.doi.org/10.1016/j.quageo.2012.07.005.

993 Shane, P., Hoverd, J., 2002. Distal record of multi-sourced tephra in Onepoto Basin,
994 Auckland, New Zealand: implications for volcanic chronology, frequency and hazards.
995 Bulletin of Volcanology, 64, 441-454.

996 Shibata, T., Yoshikawa, M., Itoh, J-I., Ujike, O., Miyishi, M., Takemura, K., 2014. Along-arc
997 geochemical variations in Quaternary magmas of northern Kyushu Island, Japan. In Gomez-
998 Tuena, A., Straub, S.M., Zellmer, G.F. (Eds). Orogenic Andesites and Crustal Growth.
999 Geological Society, London, Special Publications, 385, 15–29.

1000 Shitaoka, Y., Fukioka, T., Hasegawa, A., Kusano, T., Nagatomo, T., 2009.
1001 Thermoluminescence dating of the pyroclastic deposits of the Sanbe Volcano. Bulletin of
1002 Shimanne Nature Museum of Mt. Sambe (Sahimel),7, 15-24.

1003 Smith, V.C., Staff, R.A., Blockley, S.P.E., Bronk Ramsey, C., Nakagawa, T., Mark, D.F.,
1004 Takemura, K., Danhara, T., Suigetsu Project Members, 2013. Identification and correlation
1005 of visible tephras in the Lake Suigetsu SG06 sedimentary archive, Japan:
1006 chronostratigraphic markers for synchronising of east Asian/west Pacific palaeoclimatic
1007 records across the last 150 ka. Quaternary Science Reviews 67, 121-137.

1008 Staff, R.A., Bronk Ramsey, C., Bryant, C.L., Brock, F., Payne, R.L., Schlolaut, G., Marshall,
1009 M.H., Brauer, A., Lamb, H.F., Tarasov, P.E., Yokoyama, Y., Haraguchi, T., Gotanda, K.,
1010 Yonenobu, H., Nakagawa, T., Suigetsu 2006 Project Members, 2011. New C-14
1011 determinations from Lake Suigetsu, Japan: 12,000 to 0 cal BP. Radiocarbon 53, 511-528.

1012 Staff, R.A., Nakagawa, T., Schlolaut, G., Marshall, M.H., Brauer, A., Lamb, H.F., Bronk
1013 Ramsey, C., Bryant, C.L., Brock, F., Kitagawa, H., van der Plicht, J., Payne, R.L., Smith,
1014 V.C., Mark, D.F., MacLeod, A., Blockley, S.P.E., Schwenninger, J., Tarasov, P.E.,
1015 Haraguchi, T., Gotanda, K., Yonenobu, H., Yokoyama, Y., Suigetsu 2006 Project Members.,
1016 2013a. The multiple chronological techniques applied to the Lake Suigetsu (SG06) sediment
1017 core. Boreas, 42, 2, 259-266.

1018 Staff, R.A., Schlolaut, G., Bronk Ramsey, C., Bronk, F., Bryant, C.L., Kitagawa, H., van der
1019 Plicht, J., Marshall, M.H., Brauer, A., Lamb, H.F., Payne, R.L., Tarasov, P.E., Haraguchi, T.,
1020 Gotanda, K., Yonenobu, Y., Nakagawa, T., 2013b. Integration of the old and new Lake
1021 Suigetsu (Japan) terrestrial radiocarbon calibration data sets. Radiocarbon 55, 4, 2049-
1022 2058.

1023 Sulpizio, R., Zanchetta, G., Caron, B., Dellino, P., Mele, D., Giaccio, B., Insinga, D., Paterne,
1024 M., Siani, G., Costa, A., Macedonio, G., Santacroce, R., 2014. Volcanic ash hazards in the
1025 central Mediterranean assessed from geological data. Bulletin of Volcanology, 76, 866.

1026 Sun, S., McDonough, W.F., 1989. Chemical and isotopic systematics of 630 oceanic basalts:
1027 implications for mantle composition and processes. In: 631 A.D. Saunders, Norry, M.J.
1028 (Editor), Magmatism in Ocean Basins.

1029 Suzuki, T., Saito, H., Kasahara, A., Kuriyama, E. and Imaizumi, T. 2016. Late Quaternary
1030 tephrostratigraphy of underground sediments in the middle west part of Aizu Basin,
1031 Fukushima, northeast Japan. The Quaternary Research, 55: 1-16. (In Japanese with English
1032 abstract).

1033 Takemura, K., Iwabe, C., Hayashida, A., Danahara, T., Kitigawa, H., Haraguchi,T., Sato, T.,
1034 Ishikawa, N., 2010. Stratigraphy of marker tephras and sediments during the past 50,000
1035 years from multiple sites in Lake Biwa, Japan. The Quaternary Research, 49, 147-160 (In
1036 Japanese with English abstract).

1037 Tomlinson, E.L., Thordarson, T., Muller, W., Thirlwall, M,. Menzies, M.A., 2010.
1038 Microanalysis of tephras by LA-ICP-MS- Strategies, advantages and limitations assessed
1039 using the Thorsmork ignimbrite (Southern Iceland). Chemical Geology 279, (3-4), 73-89.

1040 Tomlinson, E.L., Albert, P.G., Wulf, S., Brown, R., Smith, V.C., Keller, J., Orsi, G., Bourne,
1041 A.J., Menzies, M.A. 2014. Age and geochemistry of tephra layers from Ischia, Italy:
1042 constraints from proximal-distal correlations with Lago Grande di Monticchio. Journal of
1043 Volcanology and Geothermal Research, 287, 22-39.

1044 Tsukui, M., 1984. Geology of Daisen Volcano. Journal of the Geological Society of Japan,
1045 90: 643-658. (In Japanese with English abstract).

1046 Wastegard, S., Veres, D., Kliem, P., Hahn., Ohlendorf, C., Zolitschka, B., The PASADO
1047 Science Team., 2013. Towards a late Quaternary Tephrochronological framework for the

southernmost part of South America – the Laguna Potrok Aike tephra record. Quaternary Science Reviews, 71, 81-90.

Wulf, S., Kraml, M., Brauer, A., Keller, J., Negendank, J.F.W., 2004. Tephrochronology of the 100 ka lacustrine sediment record of Lago Grande di Monticchio (southern Italy). Quaternary International 122, 7–30.

Wulf, S., Keller, J., Paterne, M., Mingram, J., Lauterbach, S., Opitz, S., Sottili, G., Giaccio, B., Albert, P.G., Satow, C., Tomlinson, E.L., Viccaro, M., Brauer, A., 2012. The 100-133 ka record of Italian explosive volcanism and revised tephrochronology of Lago Grande di Monticchio. Quaternary Science Reviews, 58, 104-123.

Yamamoto, T., 2017. Quantitative eruption history of Pleistocene Daisen Volcano, SW Japan. Bull. Surv. Japan, 68 (1), 1-16.

Table Captions

Table 1: Proximal eruption stratigraphy, nomenclature and age of proximal units identified at Sambe and Daisen volcanoes following Machida and Aria (2003) and other key stratigraphic interpretations. ^{14}C age estimates are quoted at 95.4% (2σ) confidence interval, some represent the integration of multiple ^{14}C dates (refer to discussion in the text) that have been combined in an OxCal model. References: [(1)] Fukuoka and Matsui (2002); [(2)] Smith et al., (2013); [(3)] Shitaoka et al., 2009; [(4)] Fukuoka, (2005); [(5)] Yamamoto, (2017); [(6)] Domitsu et al. (2002); [(7)] Katoh et al., (2007); [(8)] Machida and Arai (2003); [(9)] Kimura et al., (1999); [(10)] Hayakawa (1996). *Eruption ages derived distally based on suggested proximal-distal tephra correlations.

Table 2: Visible SG06 tephra layers linked to eruptions along the SWJA. The stratigraphic positions of the widespread tephrostratigraphic markers are shown (Kikai Akahoya, Aira Tephra Formation and Aso-4) based on correlations in Smith et al. (2013). The core sections marked in bold were sampled for chemical analysis. Composite depth of the base of the tephra is taken from the SG06 correlation model. Ages in IntCal13 yrs BP are provided for all tephra layers within the ^{14}C timeframe (<50 ka) and beyond are presented in ka (uncertainties represent either 95.4%, or 2σ). † indicates major element glass data of Smith et al., (2013) have been supplemented new analyses.

Table 3: Average major, minor, and trace element glass compositions of tephra layers in the SG06 sedimentary record which have been correlated to the SWJA (Sambe and Daisen). * denotes data that follows Smith et al. (2013) and is not supplemented by new major element data here.

Table 4: Average major, minor and trace element glass compositions of distal ash layers associated with explosive volcanism at Daisen volcano.

Table 5: Differential ages for Daisen volcano erupted Post-AT using the high-precision SG06 age-depth model (IntCal13). Median number of years are calculated between eruptions are given, along with time intervals calculated at the 68.2% (1σ) and 95.4% (2σ) confidence intervals.

Figure Captions

Figure 1: Map showing the location of Sambe and Daisen stratovolcanoes (SWJA) and Lake Suigetsu in Fukui prefecture, central Honshu, Japan. Insert: Shows all the volcanic centres that were active in the Late Quaternary along the Japanese arcs, which include large calderas on Kyushu, northern Honshu and Hokkaido. The HVZ is the Hohi Volcanic Zone. The dispersal of the largest known Plinian eruption from Late Quaternary explosive volcanism along the SWJA, the Daisen Kurayoshi Pumice (DKP) is shown and taken from Machida and Arai (2003). Other sedimentary records used or discussed are shown: red star is location of AB-12-2 borehole from Naka-iwata, Aizu-bange Town, 600 km NE of Daisen volcano; green star is location the Ichi-no-Megata (IMG) sedimentary record containing DKs ash, NW Honshu; Sea of Japan cores (GH89-2-25 and GH89-2-27) that contain the SAN1 marine tephra layer; yellow star is the location of the Lake Biwa core (BIW07-6) containing Daisen and Sambe tephra layers; and black star is core KT96-17-2 which contains the DKs (refer to text for references).

Figure 2: A-B: K_2O vs SiO_2 classification diagrams showing the compositions of all visible SG06 tephra layers, data includes newly presented major element glass data and also data from Smith et al. (2013). Proximal compositional fields are based on data presented here and in the supplementary information (Daisen, Sambe and Kuju volcano) and data published in Smith et al. (2013). Error bars represent 2 x standard deviations of repeat analyses of the StHs6/80G (Jochum et al., 2006) reference glass. **C-F:** Average Primitive Mantle normalised compositions of the thirteen SG06 tephra layers assigned to South West Japan Arc (SWJA) volcanism on the basis the present the diagnostic depletions in the Y/HREE. Proximal envelopes for the SWJA are defined based on new proximal trace element glass data generated in this investigation (**Supplementary material 1**). Primitive mantle values used for normalisation follow Sun and McDonough (1989). The proximal envelopes for the Kyushu Arc calderas (Aira, Aso, Kikai, Ata), Hokkaido and Northern Honshu Arc calderas (Toya, Shikotsu, and Towada) and the Norikura Volcanic Zone (Ontake and Takemura) are based on glass data from Kimura et al. (2015) and Maruyama et al. (2016).

Figure 3: Yttrium content of the SG06 tephra layers versus depth in the SG06 core. Thirteen of the twenty-three analysed layers are assigned to SWJA volcanism on the basis of the low Y content in their volcanic glasses. SWJA range is based on new proximal Daisen and Sambe glass data. Also shown are the ages of all the SG06 tephra layers dated using the SG06 IntCal13 age-depth model (95.4 % confidence range) in the radiocarbon timeframe (0-50 ka). Beyond this the age-depth model is extrapolated and anchored by tephra ages (e.g., Aso-4), based on previous tephra correlations to dated key tephrostratigraphic markers (Smith et al., 2013). All ages reported that are outside the ^{14}C timeframe are provided in ka with 2σ errors (equivalent to 95.4% probability range).

Figure 4: Selected major element bi-plots comparing the new and existing (Smith et al., 2013) major element glass compositions of Sambe and Daisen SG06 layers to the compositions of proximally characterised deposits (**Supplementary material**). The plots

demonstrate the significant overlap observed between the glasses erupted at the two volcanoes, but also shows the diagnostic means to distinguish them.

Figure 5: Selected bi-plots showing the trace element glass concentrations and ratios of the SG06 tephra layers, those from other key sedimentary records (**Table 4**) and proximal deposits from Daisen and Sambe (**Supplementary material 1**).

Figure 6: Major and trace element bi-plots comparing the glass compositions of Sambe SG06 tephra layers compared to the proximal glass data of Sambe eruption deposits (**Supplementary material 1**).

Figure 7: Major and trace element bi-plots comparing the glass compositions of post-AT Daisen derived SG06 tephra layers to the proximal glass data of Daisen eruptive deposits. New distal glass data is also presented from tephra layers recorded in cores from Lake Biwa (BIW07-06) and Ichi-no-Megta (IMG06) sedimentary cores (**Table 4**). Published reference data [(1)] Domitsu et al., (2002): Proximal Daisen Kusadanihara pumice (DKs) glass data and its distal equivalent recorded in the KT96-17/P-2 Sea of Japan core. All ages reported that are outside the 14C timeframe are provided in ka with 2σ errors (equivalent to 95.4% probability range).

Figure 8: Major and trace element bi-plots comparing the glass compositions of pre-AT Daisen SG06 tephra layers to melt inclusion data from plagioclase sampled from the pre-AT Daisen eruptive deposits (Furusawa, 2008). Shown are proximal matrix glass thought to relate to the DSP eruptive unit (Supplementary Material). Also included are the major element glass compositions of the Kuju Handa (Kj-Hd) pyroclatic flow. Distally the SAN1 marine tephra glass compositions following Ikehara et al. (2015), and new glass data from the equivalent layers in Sea of Japan cores (GH89-2-27 and GH89-2-25) (**Table 4**; Supplementary material). Finally the SG06 data is compared to glass data of a two distal DKP candidates; (1) TKN1080 from the Takano formation (Nagahashi et al., 2007) and (2) a distal layer (30.08-30.12m) recovered from borehole AB12-2 in Naka-iwata, Aizu-bange town 600 km north of Daisen volcano (Suzuki et al., 2016; **Table 4**). All ages reported that are outside the ^{14}C timeframe are provided in ka with 2σ errors (equivalent to 95.4% probability range).

Figure 9: The integrated proximal-distal event stratigraphy of Daisen and Sambe volcanoes based on the record preserved in the Lake Suigetsu SG06 sedimentary archive, with correlations to other sedimentary records. The SG06 tephra ages are shown as IntCal13 yrs BP in the radiocarbon timeframe (95.4 %). Beyond the annually laminated and 14C dated portion of the sequence, the age-depth model is based on a linear extrapolation that is anchored by deeper chronological tie points, which include ^{40}Ar/^{39}Ar ages of volcanic units (e.g., Aso-4/SG06-4963) All ages reported that are outside the ^{14}C timeframe are provided in ka with 2σ errors (equivalent to 95.4% probability range).

Supplementary Material 1: Proximal reference samples localities, proximal reference glasses data (major and trace element), distal SG06 glass data (major and trace element), potentially distal Daisen tephra glass data (major and trace element) and all secondary standard analyses run alongside tephra samples.

Supplementary Figure 1: CaO vs. SiO_2 bi-plots used to help assign the SWJA derived SG06 tephra layers to either Sambe or Daisen volcano on the basis of their major element glass compositions.

Supplementary Figure 2: SG06 tephra ages compared or integrated with proximal ^{14}C dating derived from charcoals extracted from with pyroclastic deposits at Daisen and Sambe volcanoes. **A:** SG06 provides more precise ages for Holocene Sambe eruptions Taihezan (Th-pd) and Shigaku (S2-fl). **B**: Ages of explosive activity occurring at Sambe at the end of the last glacial period, compared to the distal SG06-1965 and Sakate tephra recorded in the Chugoku Mountains, Western Japan. **C:** The integrated proximal-distal chronology of post-AT eruptions at Daisen volcano. References; [(1)] Fukuoka and Matsui (2002); [(2)] Katoh et al. (2007); [(3)] Matsui and Inoue (1970); [(4)] Fukuoka (2005); [(5)] Yamamoto (2017).

Supplementary Figure 3: Differential ages calculated between Daisen eruption post-AT using the high-precision SG06 age-depth model (IntCal13).

Sambe		Daisen				Dispersal	Eruption size		Age
Fukuoka and Matsui (2002)	**Machida and Arai (2003)**		Okada and Ishiga (2002)	Kimura et al. (2005)	Yamamoto (2017)		Classif.	**VEI**	**(IntCal13 yrs BP; 95.4%)**
Taihezan fl (Th-pd) (cycle VII)	Ohirasan (SOh)					ENE		4-5	3,985-4,085 [1]
Shigaku fl (S2-fl) (cycle VI)						ESE			5,330-5,590 [1]
			Kikai Akahoya (K-Ah)						*7,230-7,276 [2]
Kiriwari ash (K-fa) (cycle V)									ca. 10 ka [1]
Ukinuno ash (Uk-fa) (cycle IV)						E		-	-
Midorigaoka fl (Md-fl) (cycle IV)								-	19 ± 4 ka [3] (TL)
Ukinuno fa (Uk-pfa; U2) (cycle IV)	Ukinuno (SUP/SuK)					ESE	sub-Plinian	5	-
Oda fl (Od-fl; U1) (cycle IV)								-	19,050-19,445 [4]
Hatasedani fl (Ht-fl) (cycle IV)								-	18,880-20,790 [1]
		Kagamiganaru (DKg)						-	
			Misen pfl (MiF)		Amidagawa (Flow; AmP)	N			20,635-21,015 [5]
		Misen (DMs) (Flow & Fall)	Kusadanihara (KsP)		Kusadanihara (Fall)	N	sub-Plinian		*21,770-22,178 [6]
			Misen pumice (MsP)		Masumizuhara† (MsP; Flow)	E (W†)		4-5	*27,745-28,435 [7] 28,040-28,630 [5]
		Higashi-Daisen (DHg)	Ueno-hoki	Higashi-Daisen Pumice Fall (HgP)	Higashidaisen (Fall)	E	sub-Plinian/ Plinian	-	-
				Higashi-Daisen Ash Fall (HgA)			Vulcanian		
		Sasaganaru (DSs)	Odori (Od)	Odori Ash (OdA; Fall)	Odori (Fall) and Sasaganaru (Flow)	E (SE)	Vulcanian	5	-
			Shitano-hoki (Sh)	Sasaganaru flows (SaF; Flow) Sasaganaru (SaA; Fall)					*28,085-28,715 [7]
			Aira Tanzawa (AT)						*30,030-30,125 [2]
Ikeda pumice (Ik-pd)[1] (cycle III)	Ikeda (SI)					ESE	Plinian	5	~ 37 ka [8]
		Kamogaoka (DKg)		Kamogaoka Ash Fall (KaA)	Kamogaoka (Fall) and Makibara (Flow)				-
Ohda pumice flow [1] (cycle II)	Oda (SOd)						Plinian		~ 53 ka[8]
Unnan Pumice Fall (cycle II)	Unann (SUn)						Plinian		72 ± 13 ka[3]
		Kurayoshi (DKP)		Kurayoshi Pumice (DKP)	Kurayoshi (DKP)	E	Plinian	6	~46 or 55 ka[8]
				Hori block and ash Flow (HoF)					
		Sekigane (DSP)		Sekigane Pumice (DSP)	Sekigane (DSP)	E	Plinian	5	67 ka[5]
		Namadake (DNP)			Namadake (DNP)	E	Plinian	5-6	~80 ka[8]

Aso-4						87.5 ± 5 ka
Kiuski pfa (cycle I) Kiuski pfa (cycle I)	Kisuki (SK)		ENE	Plinian	6	~112 ka[8]; 100±20 ka[9]
		Hiruzenbara (DHP)	E	Plinian	5-6	-
		Matsue (DMP)	W	Plinian	5-6	~125 ka [10]

Table 1.

Sample (SG06-)	Bore hole A	B	C	Composite depth: Base (cm)	Thickness (cm)	Major element glass compositions n	SiO_2	K_2O	FeOt	Trace element glass concentrations (ppm) and ratio n	Y	Zr	Th	Y/Th	Zr/Th	Age ^{14}C (cal. yrs BP; 95.4% range)	Interpolated (ka) (2 sigma)	Source/Tephra correlation
588	**A-03-14**	B-03-03a		587.9	0.2	25	74.33-77.97	2.25-3.99	0.50-1.83	13	3.3-4.3	79-108	9.1-13.0	0.34 ± 0.04	8.5 ± 0.7	4,036 ± 32		Sambe- Taiheizan pd (Th-pd)
775	**A-04-13**			775.4	0.1	27	74.41-77.97	1.97-3.79	0.48-1.78		-	-	-	-	-	5,501 ± 20		Sambe - Shigaku pfl (S2-fl)
967	A-06-01	**B-05-04**	C-07-γ	**967.3**	**2.8**											**7,253 ± 46**		**Kikai-Akahoya (K-Ah)***
1965	A-11-00	**B-10-02**	-	1964.5	0.7	27'	76.19-77.43	2.41-3.96	0.65-1.19	13	2.8-5.7	48-77	8.8-13.3	0.33 ± 0.07	5.75 ± 0.8	19,551 ± 80		Sambe- Midorigaoka fl (Md-fl)
2504	**A-13-07**	B-12-150.8cm	-	2503.5	0.1	1 1'	74.43-77.74	3.08-3.88	1.10-1.60	9	3.8-8.7	82-146	8.5-10.4	0.54 ± 0.19	11.5 ± 3.0	28,449 ± 78		Daisen- Masumizuhara (MsP)
2534	A-13-08	**B-13-02**	-	2534.4	0.6	2 5	75.52-76.77	3.04-3.87	1.00-1.30	1 4	3.5-6.5	72-119	8.3-10.4	0.54 ± 0.10	9.8 ± 1.2	28,888 ± 72		Daisen- Hiashidasien pumice (HgP)
2535	A-13-156.3cm	**B-13-21.1cm**	-	2534.9	0.1	2 0	75.19-76.80	3.03-4.18	0.93-1.57		-	-	-	-	-	28,895 ± 72		Daisen- Hiashidasien Ash (HgA)
2601		**B-13-06a**		2600.6	0.2	2 5'	72.67-77.91	2.75-4.68	0.83-1.60	1 2	2.8-5.4	78-124	6.8-14.3	0.42 ± 0.06	11.4 ± 0.7	29,830 ± 96		Daisen- Odori (OdA)
2602	-	**B-13-06b**	-	2601.5	0.4	2 8	74.14-76.58	2.96-4.16	1.06-2.37	2 0	3.6-4.9	83-128	6.3-10.6	0.45 ± 0.06	12.0 ± 0.8	29,837 ± 96		Daisen- Sasaganaru (SaF)
2650	A-14-01	**B-13-Bottom**	-	**2650.3**	**35.1**											**30,078 ± 96**		**Aira Tephra Formation (AT)***
3668	A-19-04	**B-19-03**	-	3668.1	0.3	50' 4	75.54-78.54 77.62-78.09	2.63-4.89 3.11-3.49	0.41-1.00 1.20-1.40	10 5	6.7-9.2 20.8-36.3	45-65 113-131	8.9-14.1 8.9-12.2	0.66 ± 0.06 2.56 ± 0.96	5.0 ± 0.2 11.1 ± 2.0	46,295 ± 418		Sambe- Ikeda Aira
3974	-	**B-20-07**	-	3973.8	0.03	2 2	74.60-78.29	2.70-4.42	0.40-1.39	9	1.2-5.5	24-122	2.7-12.5	0.47 ± 0.09	10.7 ± 1.5		50.9 ± 0.4	Daisen- Kamogaoka (?)
4124	-	**B-21-03**	C-17-06	4124.0	0.2	1 4	76.33-77.77	3.95-4.59	0.34-0.62	1 4	6.4-8.7	21-27	4.3-6.2	1.58 ± 0.11	5.0 ± 0.5		53.8 ± 1.2	Sambe- Unnan (SUn)
4141	-	**B-21-04**	-	4141.2	1.3	4 0'	76.87-78.44	3.77-4.24	0.67-1.14	1 7	4.7-8.6	89-121	9.4-13.1	0.62 ± 0.10	9.4 ± 0.7		54.4 ± 1.6	Kuju - SAN1
4281	-	**B-22-01**	C-18-04	4280.9	0.3	1 9'	73.27-76.69	2.67-2.97	1.08-1.99	1 0	3.8-5.9	74-132	4.2-8.5	0.61 ± 0.18	13.4 ± 4.9		59.6 ± 5.4	Daisen- Kurayoshi pumice (DKP)
4318	A-23-01	**B-22-03**	-	4318.4	1.5		45.10-52.18	0.33-0.77	9.42-12.46		-	-	-	-	-		61.1 ± 5.8	Daisen Sekigane Pumice (DSP)
						2 9'	67.12-72.55	1.99-2.56	1.70-3.15	1 2	6.1-8.6	116-146	5.2-7.3	1.04 ± 0.38	21.4± 1.0		61.1 ± 5.8	Daisen Sekigane Pumice (DSP)
4963	A-28-01	**B-28-01**	C-19-03	**4962.6**	**3.5**												**87.5 ± 5 ($^{40}Ar/^{39}Ar$)**	**Aso-4***
6457	A-38-α	**B-38-07**	-	6457.0	0.1	2 4'	74.52-77.45	2.84-5.44	0.76-1.45	4	4.9-6.2	70-104	8.4-10.5	0.59 ± 0.05	9.2 ± 0.9			Daisen

Table 2.

	SG06-0588		SG06-1965		SG06-2504		SG06-2534*		SG06-2535	
	A-03-14		B-10-02		A-13-07		B-13-02		B-13-21.1cm	
wt.%	**Avg.**	**± 1σ**	**Avg.**	**± 1σ**	**Avg.**	**± 1σ**	**Avg.**	**± 1σ**	**Avg.**	**± 1σ**
SiO_2	75.80	0.98	76.88	0.34	76.37	1.20	76.28	0.31	75.94	0.39
TiO_2	0.18	0.04	0.12	0.03	0.27	0.06	0.16	0.03	0.18	0.03
Al_2O_3	13.52	0.52	13.41	0.26	12.92	0.87	13.28	0.15	13.34	0.22
FeOT	1.07	0.30	0.82	0.12	1.45	0.14	1.20	0.08	1.15	0.15
MnO	0.05	0.03	0.06	0.04	0.03	0.04	0.04	0.03	0.05	0.04
MgO	0.26	0.08	0.21	0.04	0.29	0.17	0.28	0.05	0.27	0.12
CaO	1.87	0.29	1.53	0.11	1.27	0.33	1.38	0.08	1.34	0.12
Na_2O	3.79	0.32	3.74	0.19	3.72	0.26	4.03	0.22	3.94	0.14
K_2O	3.20	0.55	3.01	0.32	3.46	0.30	3.27	0.12	3.32	0.27
P_2O_5	0.07	0.02	0.04	0.02	0.06	0.02	0.05	0.03	0.04	0.03
Cl	0.19	0.06	0.19	0.03	0.19	0.14	0.33	0.04	0.43	0.06
n	*24*		*27*		*11*		*25*		*20*	
(ppm)										
Rb	120	39	93	27	116	36	95	6	-	-
Sr	498	53	396	85	312	141	266	39	-	-
Y	3.9	0.4	3.9	0.9	5.2	1.5	5.2	1.0	-	-
Zr	95	10	65	9	111	25	93	14	-	-
Nb	12.7	1.0	12.8	1.5	11.1	0.7	12.3	2.1	-	-
Ba	778	125	771	63	568	161	623	70	-	-
La	31.3	2.5	28.0	2.8	23.2	1.2	21.7	2.4	-	-
Ce	53.5	3.5	50.6	6.3	42.3	2.6	40.2	3.4	-	-
Pr	4.4	0.4	4.4	0.5	3.9	0.4	3.7	0.3	-	-
Nd	13.4	1.1	12.2	1.2	12.7	1.4	11.4	1.2	-	-
Sm	1.2	0.3	1.3	0.2	1.8	0.4	1.5	0.1	-	-
Eu	0.4	0.1	0.4	0.1	0.4	0.1	0.4	0.1	-	-
Gd	0.9	0.3	0.8	0.2	1.2	0.3	1.0	0.2	-	-
Dy	0.6	0.2	0.6	0.1	0.9	0.3	0.8	0.3	-	-
Er	0.4	0.1	0.4	0.1	0.5	0.2	0.5	0.1	-	-
Yb	0.4	0.2	0.5	0.1	0.6	0.1	0.5	0.2	-	-
Hf	2.4	0.3	2.0	0.2	2.9	0.6	2.6	0.4	-	-
Ta	0.9	0.2	0.9	0.1	0.8	0.1	0.7	0.2	-	-
Th	11.3	1.1	11.4	1.1	9.7	0.8	9.5	0.7	-	-
U	2.8	0.3	2.9	0.2	2.8	0.3	2.7	0.2	-	-
Y/Th	0.34	0.04	0.33	0.07	0.54	0.19	0.54	0.10	-	-
Zr/Th	8.5	0.7	5.8	0.8	11.5	3.0	9.8	1.2	-	-
n	*13*		*13*		*9*		*14*		-	

Table 3

SG06-2601		SG06-2602*		SG06-3668 (Pop. 1)		SG06-3668 (Pop. 2)*		SG06-3974*	
B-13-06a		B-13-06b		B-13-06b		B-13-06b		B-20-07	
Avg.	**± 1σ**	**Avg.**	**± 1σ**	**Avg.**	**± 1σ**	**Avg.**	**± 1σ**	**Avg.**	**± 1σ**
75.84	1.39	75.63	0.47	77.62	0.71	77.89	0.15	76.65	0.79
0.19	0.05	0.18	0.04	0.08	0.03	0.13	0.04	0.13	0.04
13.37	1.01	13.57	0.20	12.79	0.54	12.25	0.10	13.16	0.55
1.13	0.23	1.54	0.46	0.63	0.20	1.33	0.06	0.89	0.22
0.05	0.03	0.06	0.02	0.07	0.04	0.04	0.02	0.05	0.03
0.21	0.15	0.34	0.17	0.11	0.07	0.14	0.01	0.18	0.17
1.26	0.38	1.42	0.15	1.13	0.27	1.11	0.06	1.20	0.27
4.14	0.46	4.04	0.28	3.75	0.38	3.82	0.12	4.15	0.36
3.49	0.50	3.42	0.48	3.58	0.53	3.31	0.16	3.38	0.44
0.05	0.02	0.05	0.01	0.02	0.02	-	-	0.05	0.02
0.28	0.11	0.28	0.04	0.22	0.09	-	-	0.28	0.08
25		*28*		*50*		*4*		*22*	
117	59	97	19	100	36	233	153	85	39
345	151	294	24	288	151	81	8	238	52
4.0	0.8	4.2	0.5	7.8	0.8	27.4	7.0	3.6	1.8
106	14	110	11	59	6	120	7	73	34
11.8	2.1	11.3	1.8	15.2	1.7	11.0	4.7	9.1	3.8
656	84	594	77	803	61	790	348	482	194
22.7	2.7	21.7	2.0	27.1	2.3	22.4	5.3	16.1	7.1
41.6	5.5	39.2	3.3	50.9	6.0	48.2	8.8	29.1	12.3
3.8	0.5	3.5	0.5	4.7	0.4	5.0	0.7	2.8	1.2
11.9	2.8	11.7	1.4	15.4	1.8	21.8	2.5	11.1	0.4
1.6	0.3	1.6	0.2	2.1	0.6	4.2	0.6	1.6	0.1
0.4	0.1	0.4	0.0	0.4	0.1	0.9	0.4	0.4	0.1
1.0	0.2	1.0	0.2	1.5	0.3	4.3	1.1	1.0	0.0
0.7	0.2	0.7	0.1	1.3	0.2	4.7	1.3	0.7	0.0
0.4	0.1	0.4	0.1	0.8	0.1	2.8	0.6	0.4	0.1
0.5	0.1	0.5	0.1	0.8	0.2	3.0	0.4	0.4	0.0
2.7	0.4	2.9	0.4	2.1	0.2	3.3	0.3	2.2	0.9
0.7	0.1	0.8	0.1	1.3	0.2	0.9	0.2	0.6	0.3
9.3	1.3	9.2	1.0	11.9	1.4	11.1	1.4	7.0	3.6
2.7	0.5	2.6	0.3	3.7	0.4	4.5	2.1	2.1	1.0
0.42	0.06	0.45	0.06	0.66	0.06	2.56	0.96	0.47	0.09
11.4	0.7	12.0	0.8	5.0	0.2	11.0	2.0	10.7	1.5
12		*20*		*10*		*5*		*9*	

1193

1194 **Table 3 continued**

SG06-4124*		SG06-4141		SG06-4281		SG06-4318		SG06-6457	
B-21-03		B-21-04		B-22-01		B-22-03		B-38-07	
Avg.	± 1σ	Avg.	± 1σ	Avg.	± 1σ	Avg.	± 1σ	Avg.	± 1σ
76.79	0.36	77.67	0.33	74.60	1.20	70.14	1.17	76.72	0.55
0.04	0.02	0.20	0.04	0.21	0.04	0.34	0.05	0.15	0.06
13.56	0.23	12.34	0.16	14.17	0.50	15.79	0.38	13.06	0.30
0.49	0.07	0.96	0.11	1.55	0.26	2.56	0.38	1.02	0.15
0.09	0.05	0.05	0.04	0.04	0.04	0.06	0.03	0.05	0.05
0.09	0.02	0.21	0.03	0.41	0.07	0.86	0.21	0.22	0.12
0.57	0.04	1.17	0.11	1.76	0.24	2.81	0.35	1.23	0.23
3.97	0.11	3.24	0.13	4.23	0.24	4.69	0.21	3.75	0.31
4.28	0.17	3.95	0.12	2.80	0.12	2.34	0.12	3.52	0.82
0.05	0.01	0.03	0.02	0.07	0.03	0.13	0.03	0.04	0.02
0.07	0.03	0.18	0.03	0.29	0.04	0.29	0.04	0.24	0.07
14		*40*		*19*		*29*		*24*	
105	7	124	13	75	9	73	8	92	15
70	13	177	13	425	173	493	30	202	12
7.6	0.8	6.7	1.1	4.5	0.8	7.0	1.0	5.6	0.7
25	3	102	8	118	17	129	9	89	15
16.8	1.4	11.4	1.6	8.2	1.5	9.8	1.6	10.6	1.4
709	85	877	53	560	64	549	39	544	43
4.5	1.8	21.1	1.3	17.5	2.5	20.1	1.4	20.0	2.7
10.4	3.3	37.7	3.0	33.4	4.9	39.3	2.6	38.6	3.3
1.1	0.3	3.5	0.3	3.4	0.6	3.8	0.3	3.4	0.3
3.6	0.5	11.3	1.5	11.2	1.6	13.5	1.4	10.5	1.3
1.0	0.1	1.9	0.3	1.4	0.4	2.6	0.3	<LOD	-
0.2	0.0	0.4	0.0	0.5	0.0	0.7	0.2	<LOD	-
0.8	0.1	1.2	0.2	1.0	0.6	2.2	0.1	<LOD	-
1.2	0.2	1.0	0.2	1.0	0.2	1.6	0.2	<LOD	-
0.7	0.1	0.8	0.1	0.5	0.1	1.0	0.4	<LOD	-
0.8	0.1	0.8	0.0	0.6	0.1	2.0	2.2	<LOD	-
1.2	0.2	2.9	0.3	2.9	0.5	3.4	0.4	2.6	0.5
1.5	0.1	0.9	0.1	0.5	0.3	0.6	0.1	0.7	0.1
5.0	0.5	11.0	0.9	7.2	1.2	6.1	0.6	9.6	0.9
3.8	0.3	2.5	0.4	2.8	0.5	1.9	0.3	2.8	0.6
1.51	0.11	0.62	0.10	0.61	0.18	1.04	0.38	0.59	0.05
5.0	0.5	9.4	0.7	13.4	4.9	21.4	1.0	9.2	0.9
14		*17*		*10*		*12*		*4*	

Table 3 Continued

	BIW07-06		BIW07-06		BIW07-06		BIW07-06	
	5.59m		8.84-8.87m		9.370-9.385 (2 layers)		16.02-16.04	
wt.%	Avg.	± 1σ	Avg.	± 1σ	Avg.	± 1σ	Avg.	± 1σ
SiO_2	76.82	0.23	75.77	0.96	75.88	1.41	76.74	0.17
TiO_2	0.12	0.03	0.19	0.05	0.16	0.06	0.09	0.03
Al_2O_3	13.24	0.11	13.39	0.39	13.38	0.96	13.49	0.16
FeOT	0.98	0.10	1.30	0.27	1.30	0.17	0.80	0.07
MnO	0.05	0.04	0.03	0.03	0.06	0.03	0.05	0.03
MgO	0.24	0.03	0.28	0.10	0.26	0.14	0.18	0.02
CaO	1.56	0.09	1.41	0.24	1.37	0.33	1.44	0.08
Na_2O	3.84	0.13	4.04	0.14	3.96	0.40	4.07	0.11
K_2O	2.90	0.20	3.31	0.22	3.40	0.38	2.99	0.12
P_2O_5	0.04	0.02	0.05	0.03	0.05	0.03	0.03	0.02
Cl	0.20	0.04	0.23	0.18	0.18	0.14	0.12	0.07
n	*15*		*14*		*25*		*11*	
(ppm)								
Rb	86	6	105	13	116	25	138	55
Sr	434	41	307	30	288	34	134	116
Y	3.5	0.4	5.0	1.0	4.0	0.3	8.0	1.3
Zr	75	7	105	20	109	4	34	14
Nb	12.2	1.1	11.1	0.7	10.9	0.6	16.8	7.8
Ba	811	56	649	18	609	56	721	232
La	29.0	2.8	22.9	0.6	22.8	0.9	10.2	8.7
Ce	50.4	4.1	42.0	1.4	41.2	1.6	21.4	16.3
Pr	4.4	0.4	3.8	0.1	3.7	0.2	1.9	1.3
Nd	13.0	1.2	12.7	0.9	11.8	0.6	7.8	4.9
Sm	1.5	0.2	1.8	0.3	1.6	0.1	1.4	0.6
Eu	0.4	0.0	0.5	0.1	0.4	0.0	0.3	0.1
Gd	1.0	0.1	1.3	0.2	0.9	0.1	1.3	0.5
Dy	0.6	0.1	0.9	0.2	0.7	0.1	1.4	0.3
Er	0.3	0.0	0.5	0.1	0.4	0.0	0.8	0.1
Yb	0.5	0.1	0.5	0.2	0.5	0.1	1.0	0.1
Hf	2.2	0.1	2.8	0.5	2.8	0.2	1.5	0.5
Ta	0.9	0.1	0.8	0.0	0.8	0.0	1.4	0.6
Th	11.0	1.3	9.3	0.7	9.9	0.6	7.4	2.3
U	2.7	0.2	2.7	0.2	2.7	0.2	3.9	1.2
Y/Th	0.32	0.03	0.54	0.15	0.41	0.02	1.18	0.44
Zr/Th	7.0	1.1	11.4	2.8	11.0	0.6	4.5	0.7
n	*9*		*6*		*9*		*5*	

1197

1198 **Table 4**

AB-12-2		IMG06		GH89-2-27		GH89-2-25	
30.08-30.12m		16.35m		377-379cm		16.35m	
Avg.	± 1σ	Avg.	± 1σ	Avg.	± 1σ	Avg.	± 1σ
75.48	1.50	71.37	1.97	77.14	0.32	77.31	0.27
0.21	0.06	0.27	0.06	0.20	0.03	0.20	0.03
13.54	0.76	15.71	0.90	12.69	0.17	12.58	0.20
1.37	0.35	1.88	0.54	1.02	0.06	1.01	0.07
0.05	0.04	0.10	0.06	0.05	0.04	0.07	0.06
0.50	0.45	0.67	0.33	0.22	0.02	0.21	0.03
1.62	0.34	2.19	0.56	1.30	0.07	1.28	0.07
4.10	0.30	4.66	0.29	3.22	0.19	3.21	0.13
2.79	0.28	2.79	0.29	3.95	0.08	3.94	0.08
0.05	0.03	0.14	0.04	0.03	0.02	0.03	0.02
0.30	0.06	0.22	0.03	0.17	0.02	0.18	0.02
10		*16*		*21*		*15*	
84	6	90	10	-	-	-	-
382	112	451	201	-	-	-	-
4.1	0.6	6.0	0.9	-	-	-	-
113	13	154	21	-	-	-	-
7.7	0.6	10.8	1.6	-	-	-	-
546	42	625	53	-	-	-	-
18.2	1.5	24.0	2.8	-	-	-	-
33.2	2.9	45.3	5.3	-	-	-	-
3.2	0.3	4.3	0.6	-	-	-	-
10.4	1.1	14.7	2.6	-	-	-	-
1.5	0.3	2.2	0.6	-	-	-	-
0.4	0.1	0.6	0.1	-	-	-	-
1.0	0.2	1.4	0.3	-	-	-	-
0.7	0.1	1.0	0.2	-	-	-	-
0.5	0.1	0.6	0.1	-	-	-	-
0.5	0.1	0.7	0.2	-	-	-	-
2.8	0.4	3.3	0.6	-	-	-	-
0.5	0.1	0.8	0.2	-	-	-	-
6.6	0.7	6.8	1.1	-	-	-	-
2.2	0.2	2.1	0.3	-	-	-	-
0.62	0.09	0.90	0.19	-	-	-	-
17.1	2.0	23.0	2.8	-	-	-	-
12		*19*		-		-	

Table 4 continued

From	To	SG06 Differential Ages- IntCal13 yrs		
		Median	68.2% range	95.4% range
SG06-2534	SG06-2504	438	398 - 475	363 - 516
SG06-2535	SG06-2534	5	0 - 8	0 - 17
SG06-2601	SG06-2535	932	880 - 983	830 - 1036
SG06-2602	SG06-2601	6	1 - 10	0 - 20
SG06-2650	SG06-2602	246	132 - 185	185 - 312

1201

1202 **Table 5**

1203

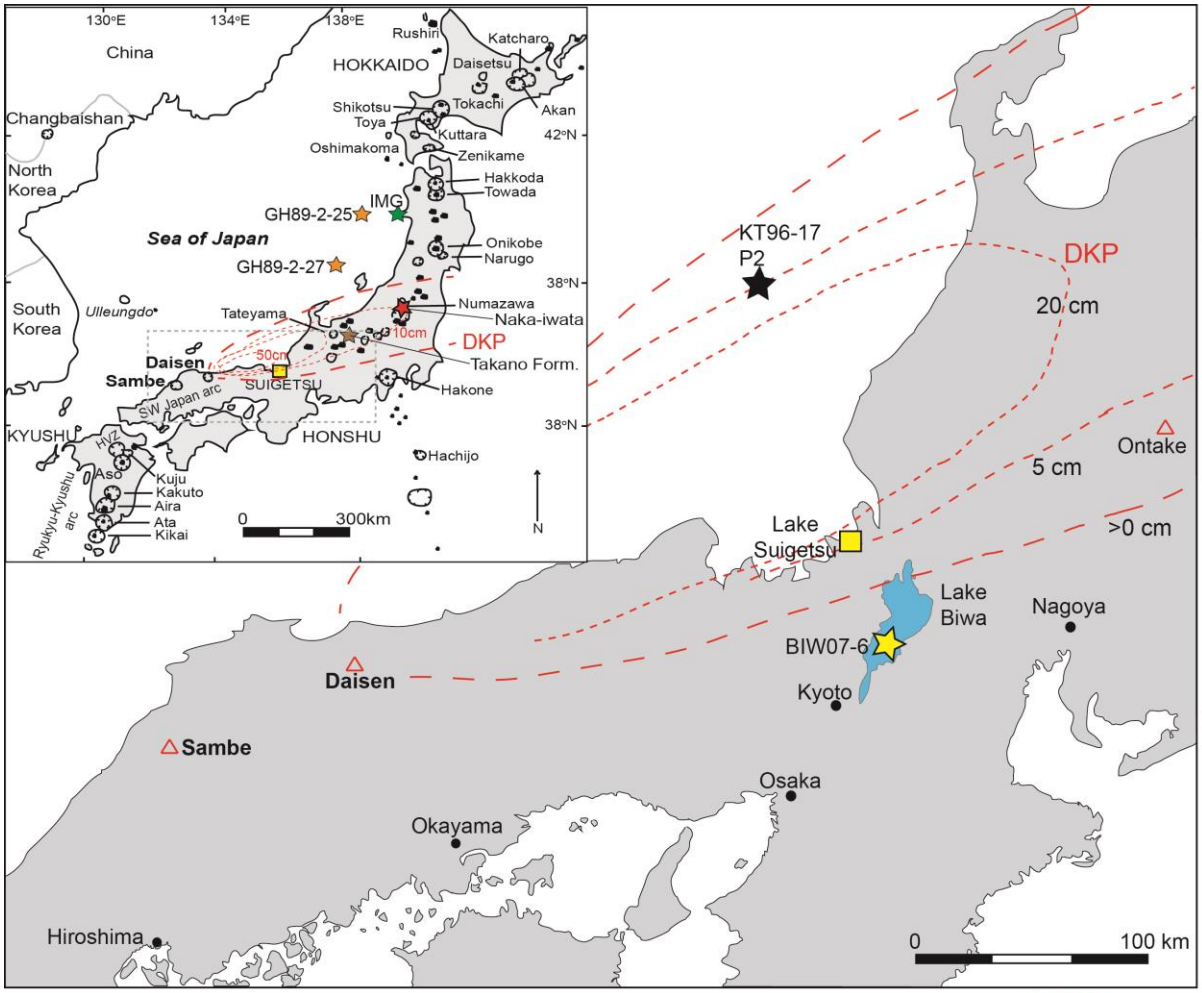

1204 Figure 1

1205 **Figure 1**

1206

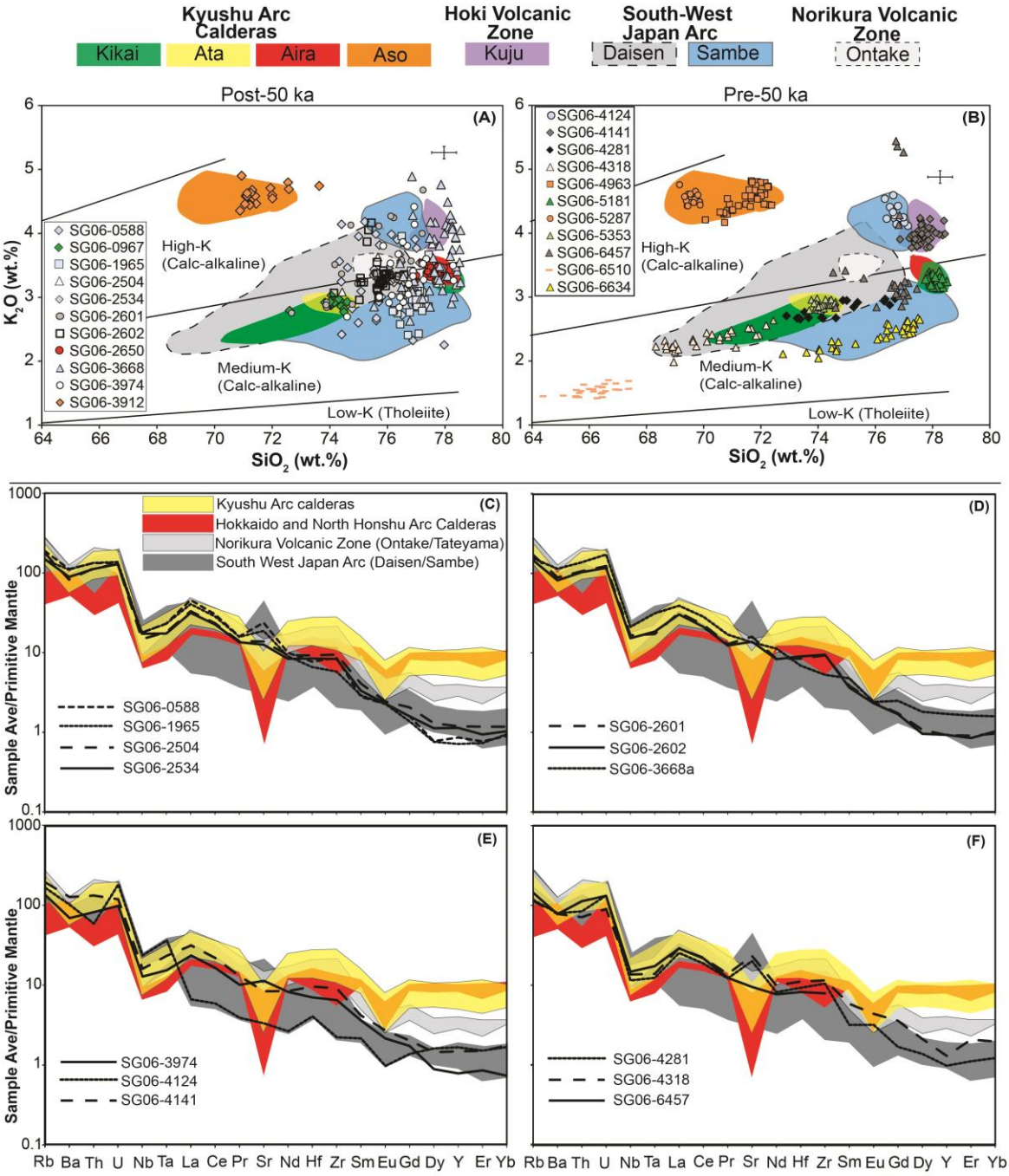

1207

1208 **Figure 2**

1209

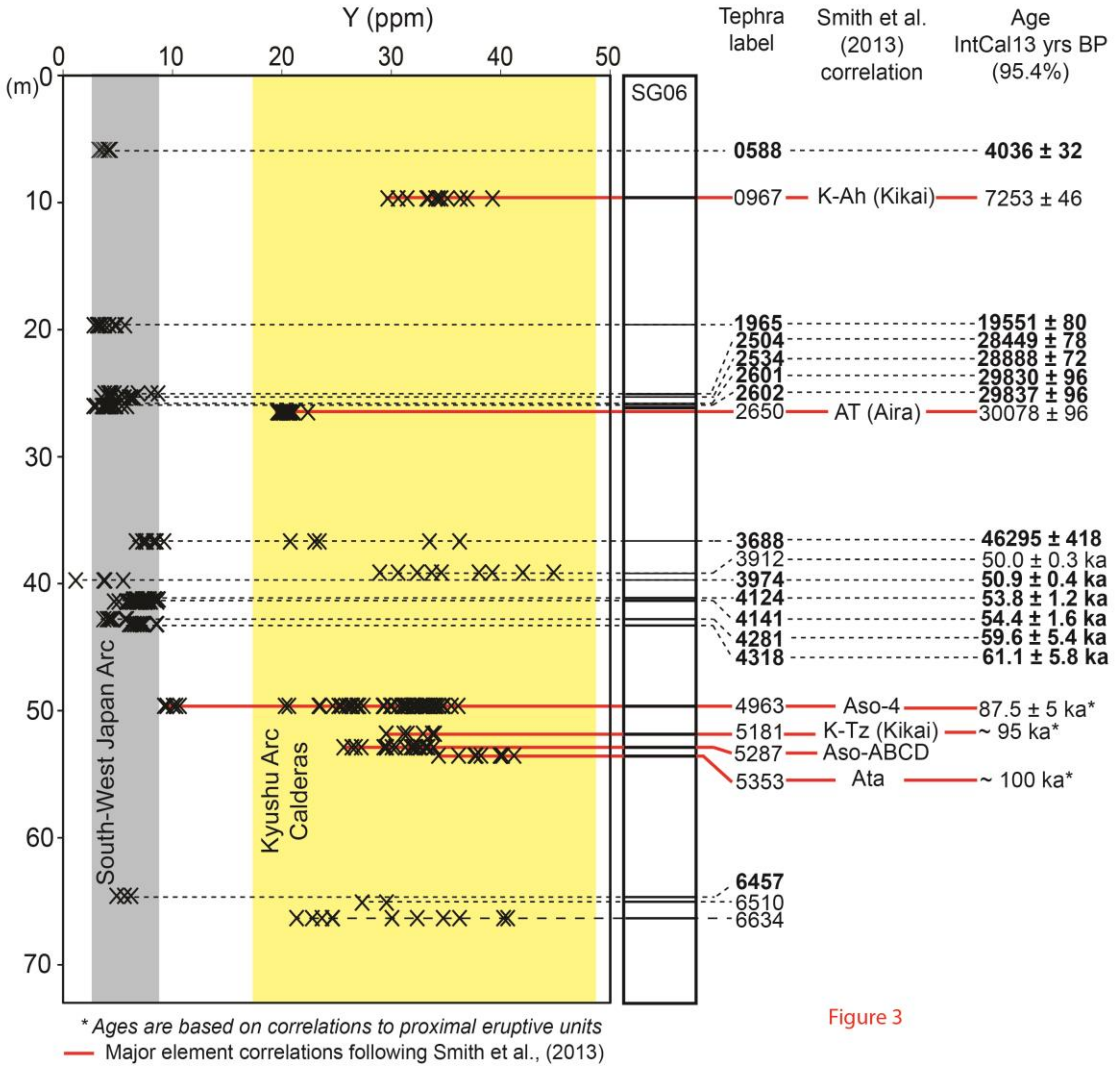

1210

1211 **Figure 3**

1212

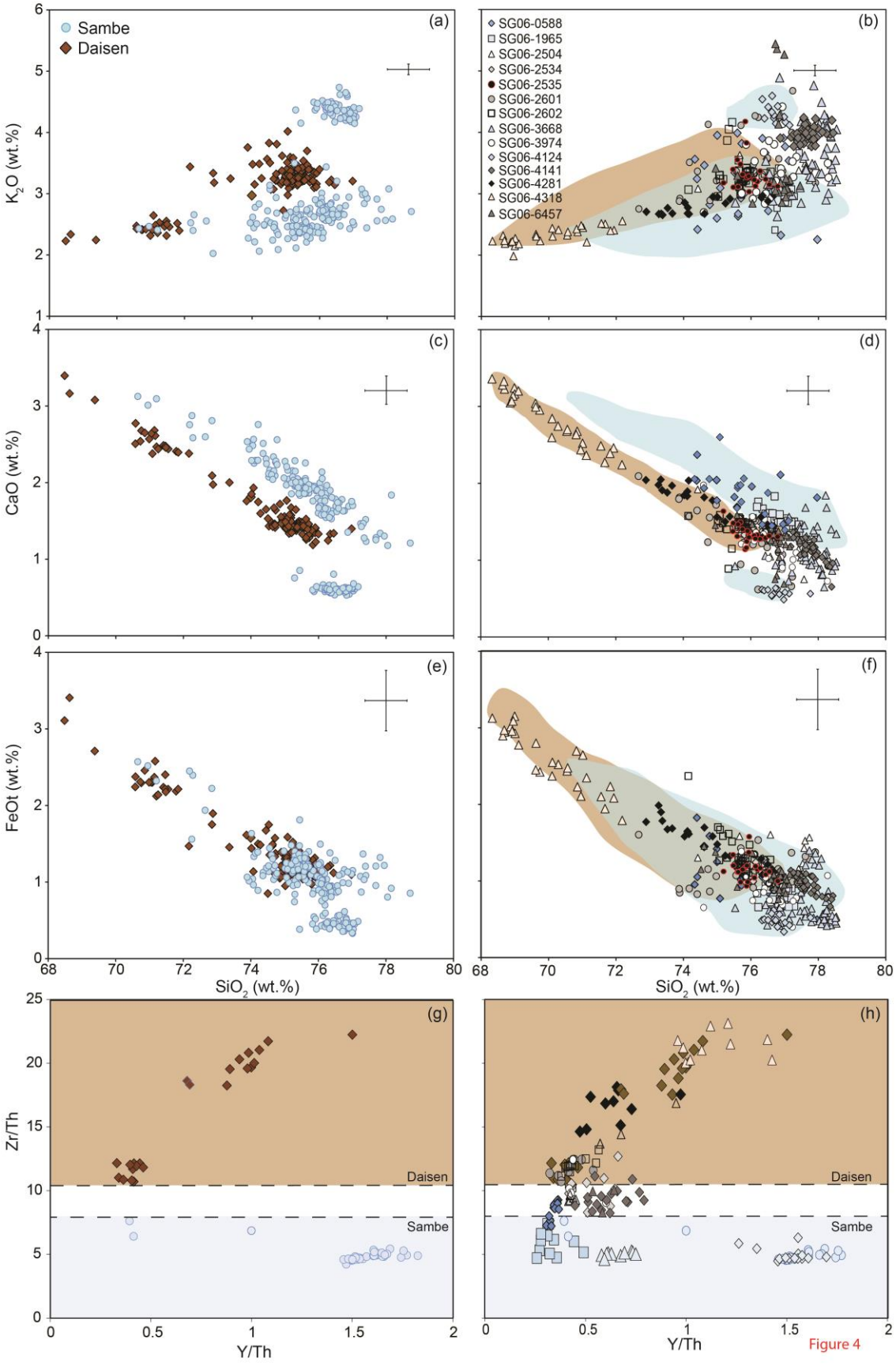

1213

1214 **Figure 4**

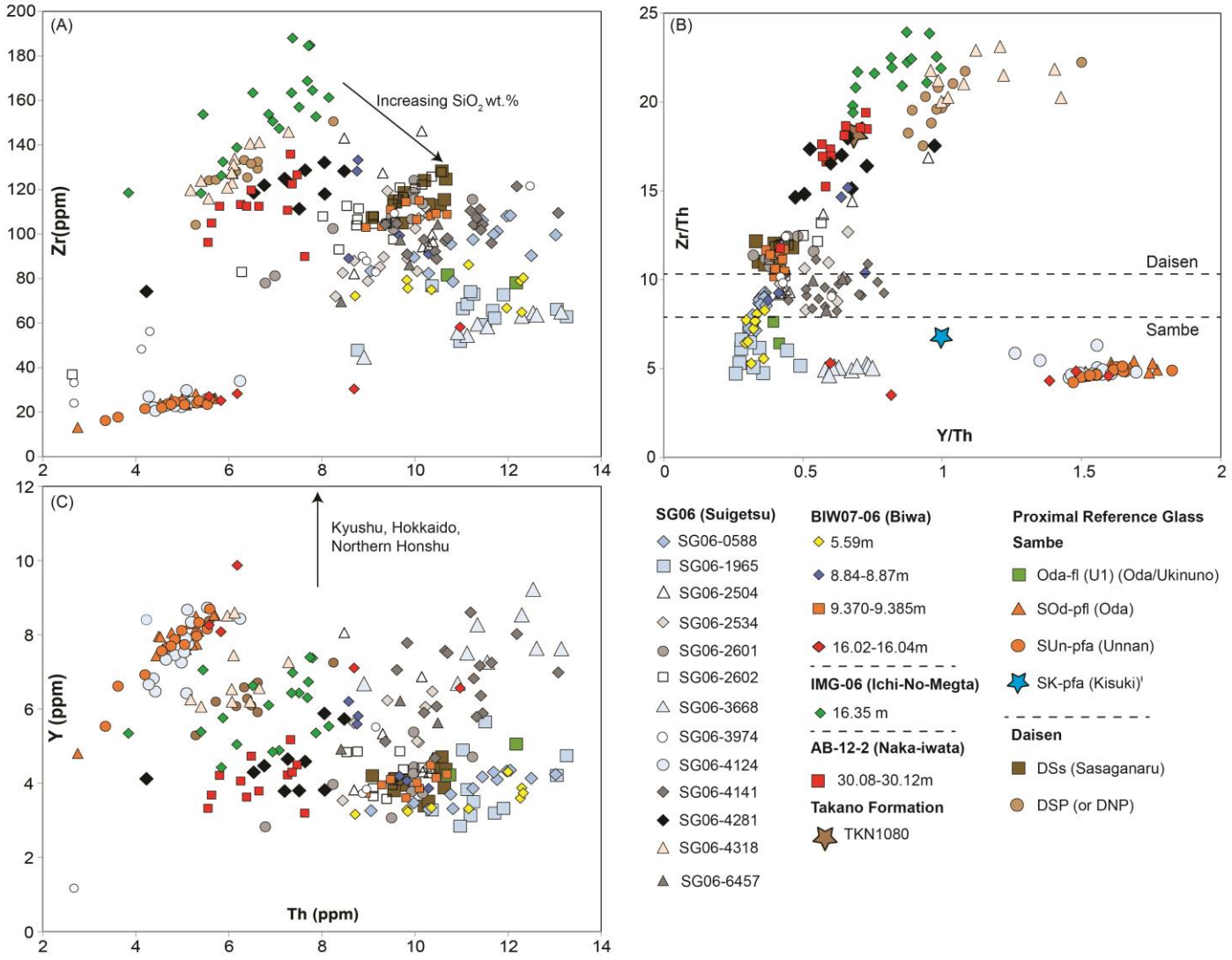
(A)
Increasing SiO2 wt.%
Zr(ppm)
(B)
Zr/Th
Y/Th
Daisen
Sambe
(C)
Kyushu, Hokkaido,
Northern Honshu
Y (ppm)
Th (ppm)
SG06 (Suigetsu)
SG06-0588
SG06-1965
SG06-2504
SG06-2534
SG06-2601
SG06-2602
SG06-3668
SG06-3974
SG06-4124
SG06-4141
SG06-4281
SG06-4318
SG06-6457
BIW07-06 (Biwa)
5.59m
8.84-8.87m
9.370-9.385m
16.02-16.04m
IMG-06 (Ichi-No-Megta)
16.35 m
AB-12-2 (Naka-iwata)
30.08-30.12m
Takano Formation
TKN1080
Proximal Reference Glass
Sambe
Oda-fl (U1) (Oda/Ukinuno)
SOd-pfl (Oda)
SUn-pfa (Unnan)
SK-pfa (Kisuki)'
Daisen
DSs (Sasaganaru)
DSP (or DNP)

Figure 5

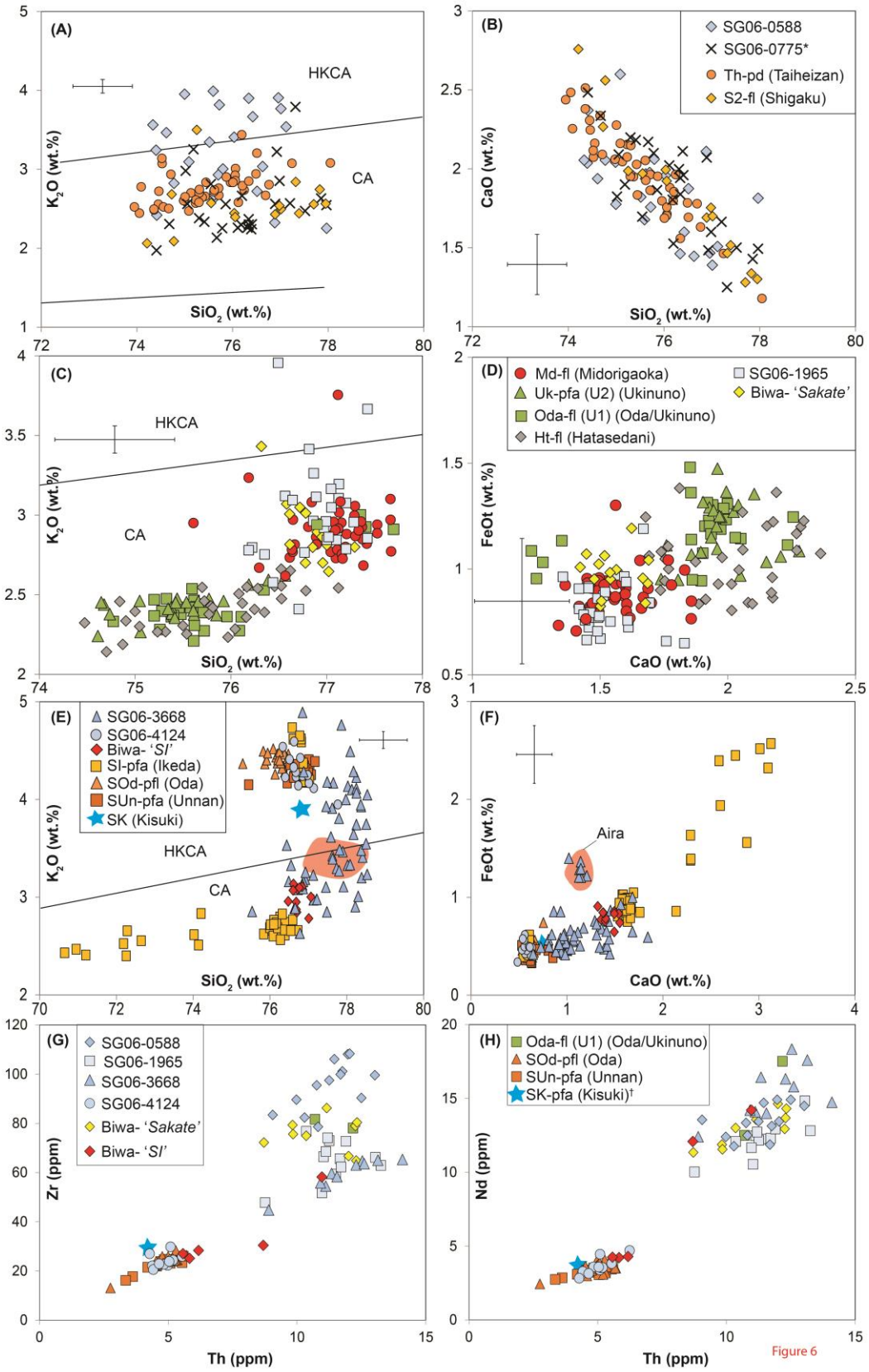

1217

1218 **Figure 6**

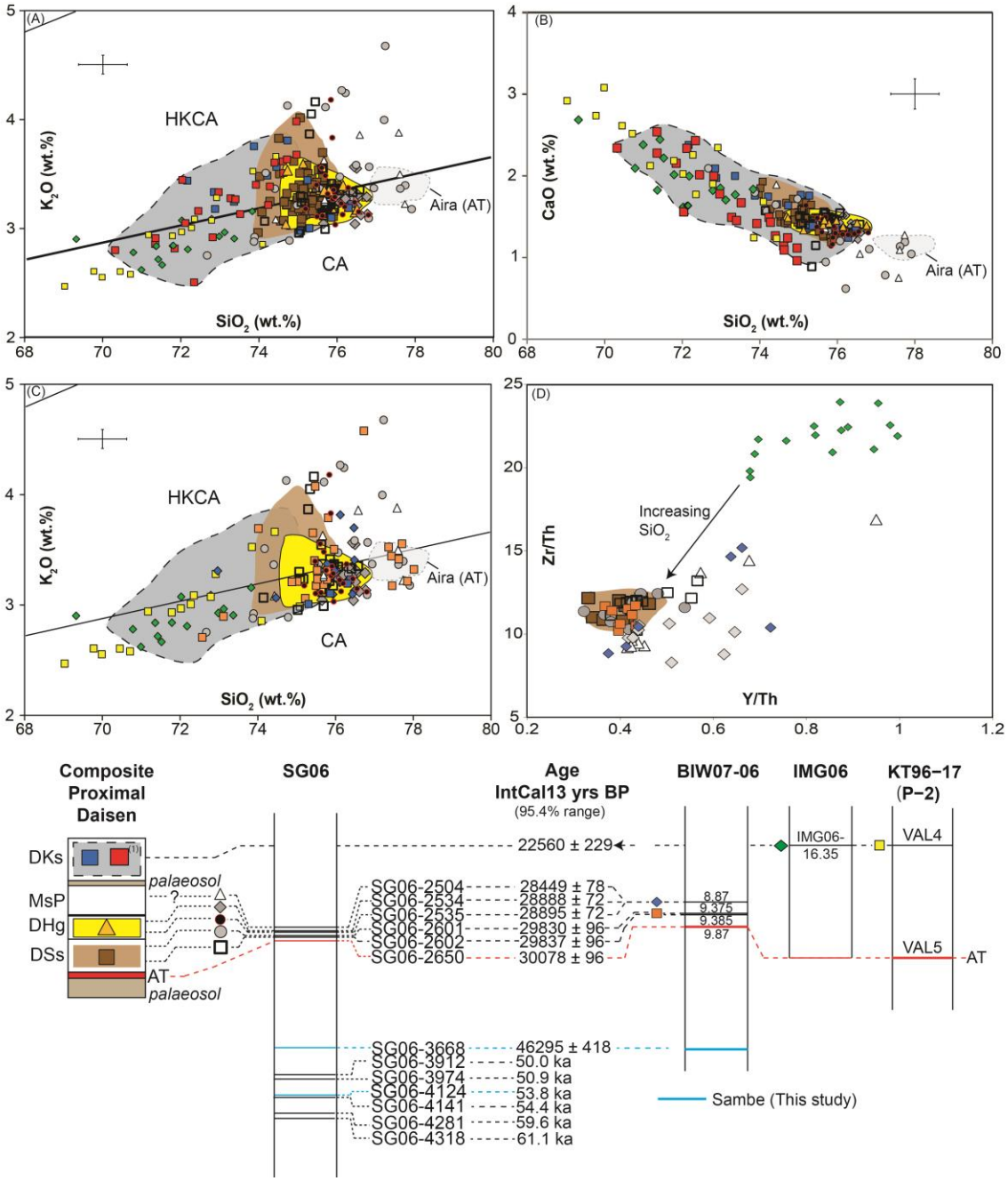
(A)
HKCA
CA
Aira (AT)
K2O (wt.%)
SiO2 (wt.%)
(B)
CaO (wt.%)
SiO2 (wt.%)
Aira (AT)
(C)
HKCA
CA
Aira (AT)
K2O (wt.%)
SiO2 (wt.%)
(D)
Increasing SiO2
Zr/Th
Y/Th
Composite Proximal Daisen
SG06
Age IntCal13 yrs BP (95.4% range)
BIW07-06
IMG06
KT96-17 (P-2)
DKs
MsP
DHg
DSs
palaeosol
?
AT
palaeosol
22560 ± 229
SG06-2504 28449 ± 78
SG06-2534 28888 ± 72
SG06-2535 28895 ± 72
SG06-2601 29830 ± 96
SG06-2602 29837 ± 96
SG06-2650 30078 ± 96
8.87
9.375
9.385
9.87
IMG06-16.35
VAL4
VAL5
AT
SG06-3668 46295 ± 418
SG06-3912 50.0 ka
SG06-3974 50.9 ka
SG06-4124 53.8 ka
SG06-4141 54.4 ka
SG06-4281 59.6 ka
SG06-4318 61.1 ka
Sambe (This study)

Figure 7

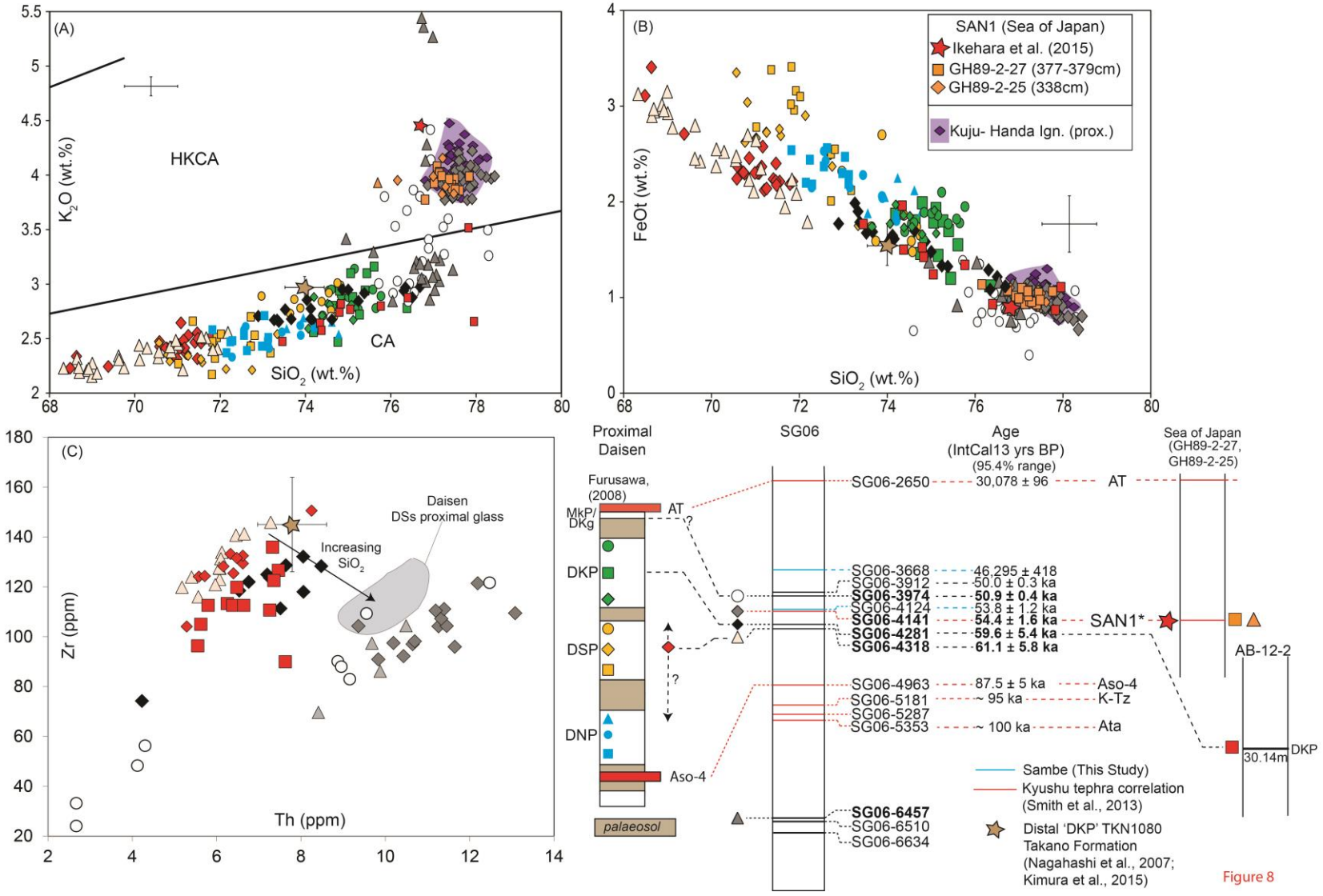
(A)
HKCA
CA
K2O (wt.%)
SiO2 (wt.%)
(B)
SAN1 (Sea of Japan)
Ikehara et al. (2015)
GH89-2-27 (377-379cm)
GH89-2-25 (338cm)
Kuju- Handa Ign. (prox.)
FeOt (wt.%)
SiO2 (wt.%)
(C)
Daisen
DSs proximal glass
Increasing
SiO2
Zr (ppm)
Th (ppm)
Proximal
Daisen
SG06
Age
(IntCal13 yrs BP)
(95.4% range)
Sea of Japan
(GH89-2-27,
GH89-2-25)
Furusawa,
(2008)
MkP/
DKg
AT
DKP
DSP
DNP
Aso-4
palaeosol
SG06-2650
30,078 ± 96
SG06-3668
46,295 ± 418
SG06-3912
50.0 ± 0.3 ka
SG06-3974
50.9 ± 0.4 ka
SG06-4124
53.8 ± 1.2 ka
SG06-4141
54.4 ± 1.6 ka
SG06-4281
59.6 ± 5.4 ka
SG06-4318
61.1 ± 5.8 ka
SG06-4963
87.5 ± 5 ka
SG06-5181
~ 95 ka
SG06-5287
SG06-5353
~ 100 ka
SG06-6457
SG06-6510
SG06-6634
SAN1*
Aso-4
K-Tz
Ata
AB-12-2
30.14m
DKP
Sambe (This Study)
Kyushu tephra correlation
(Smith et al., 2013)
Distal 'DKP' TKN1080
Takano Formation
(Nagahashi et al., 2007;
Kimura et al., 2015)
Figure 8

Figure 8

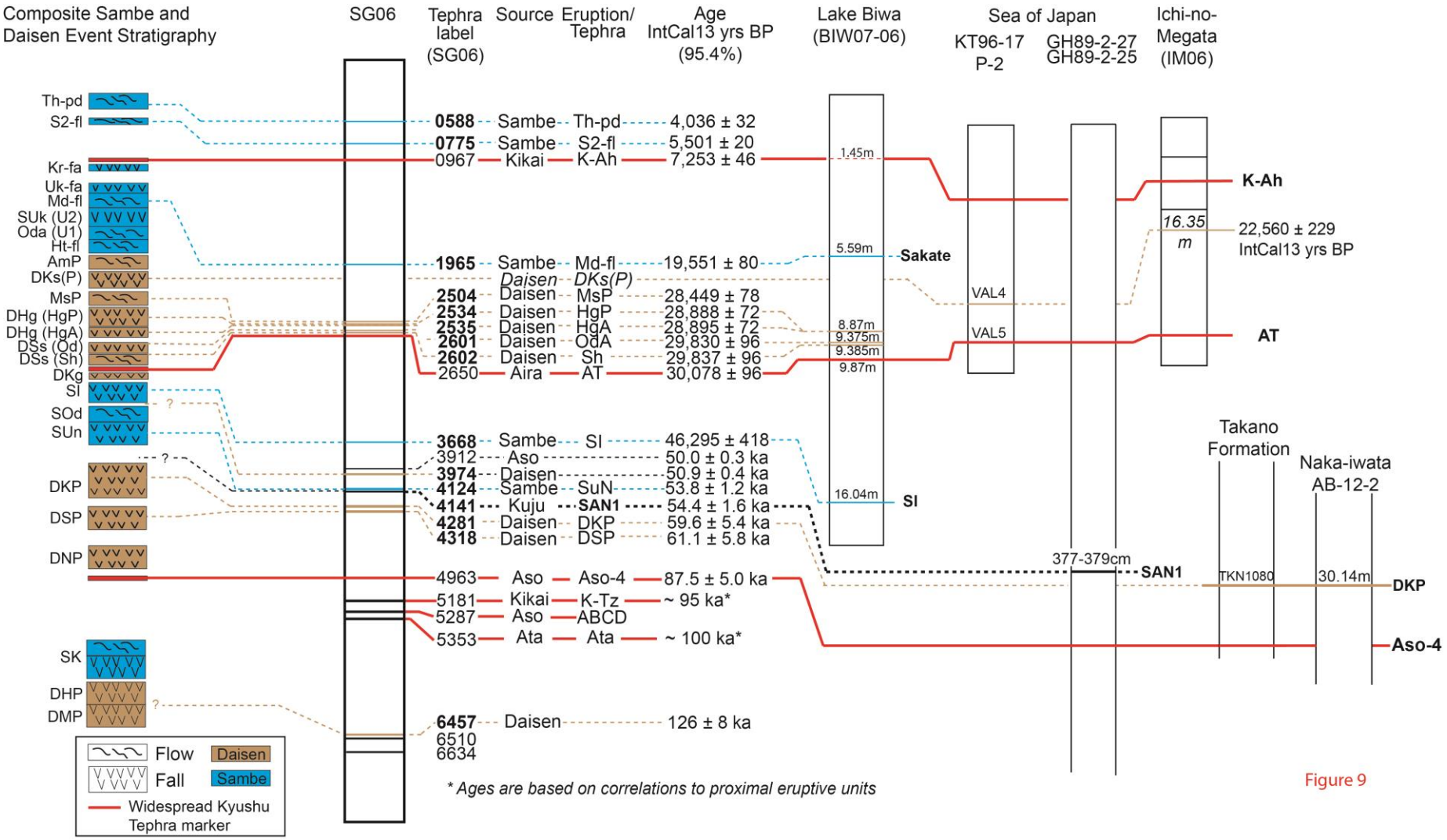
Composite Sambe and Daisen Event Stratigraphy
SG06
Tephra label (SG06)
Source
Eruption/ Tephra
Age IntCal13 yrs BP (95.4%)
Lake Biwa (BIW07-06)
Sea of Japan
KT96-17 P-2
GH89-2-27 GH89-2-25
Ichi-no-Megata (IM06)
Th-pd
S2-fl
Kr-fa
Uk-fa
Md-fl
SUk (U2)
Oda (U1)
Ht-fl
AmP
DKs(P)
MsP
DHg (HgP)
DHg (HgA)
DSs (Od)
DSs (Sh)
DKg
Sl
SOd
SUn
DKP
DSP
DNP
SK
DHP
DMP
0588 Sambe Th-pd 4,036 ± 32
0775 Sambe S2-fl 5,501 ± 20
0967 Kikai K-Ah 7,253 ± 46
1965 Sambe Md-fl 19,551 ± 80
Daisen DKs(P)
2504 Daisen MsP 28,449 ± 78
2534 Daisen HgP 28,888 ± 72
2535 Daisen HgA 28,895 ± 72
2601 Daisen OdA 29,830 ± 96
2602 Daisen Sh 29,837 ± 96
2650 Aira AT 30,078 ± 96
3668 Sambe Sl 46,295 ± 418
3912 Aso 50.0 ± 0.3 ka
3974 Daisen 50.9 ± 0.4 ka
4124 Sambe SuN 53.8 ± 1.2 ka
4141 Kuju SAN1 54.4 ± 1.6 ka
4281 Daisen DKP 59.6 ± 5.4 ka
4318 Daisen DSP 61.1 ± 5.8 ka
4963 Aso Aso-4 87.5 ± 5.0 ka
5181 Kikai K-Tz ~ 95 ka*
5287 Aso ABCD
5353 Ata Ata ~ 100 ka*
6457 Daisen 126 ± 8 ka
6510
6634
1.45m
5.59m
Sakate
8.87m
9.375m
9.385m
9.87m
16.04m
Sl
VAL4
VAL5
16.35 m
K-Ah
22,560 ± 229 IntCal13 yrs BP
AT
377-379cm
SAN1
Takano Formation
Naka-iwata AB-12-2
TKN1080
30.14m
DKP
Aso-4
Flow
Daisen
Fall
Sambe
Widespread Kyushu Tephra marker
* Ages are based on correlations to proximal eruptive units
Figure 9

Figure 9

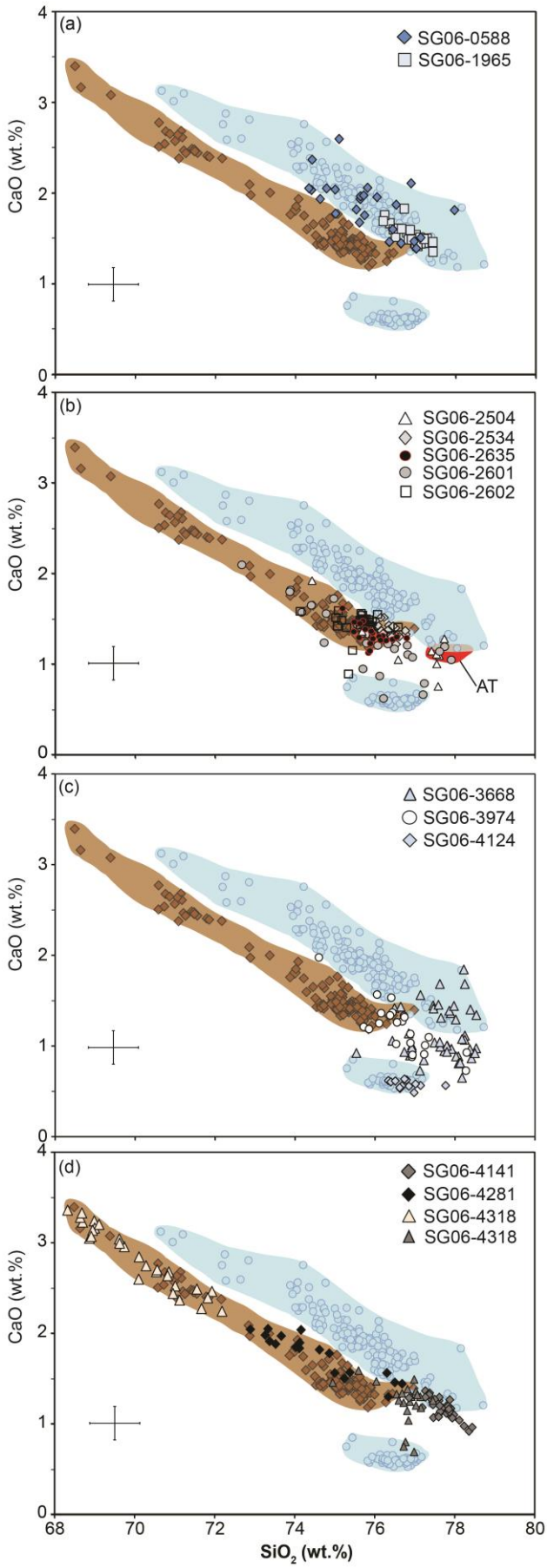

Supplementary Figure 1

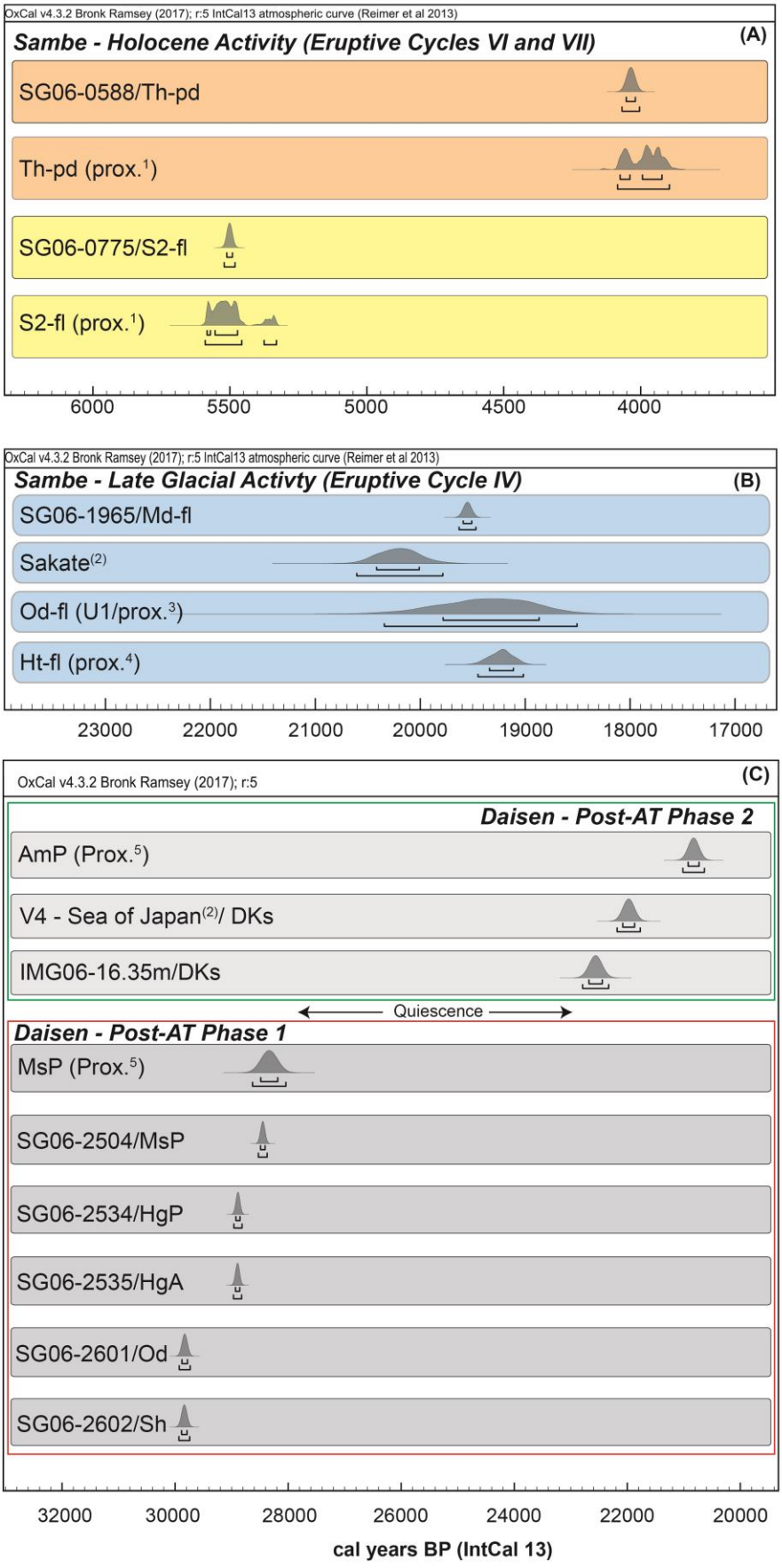

Supplementary Figure 2

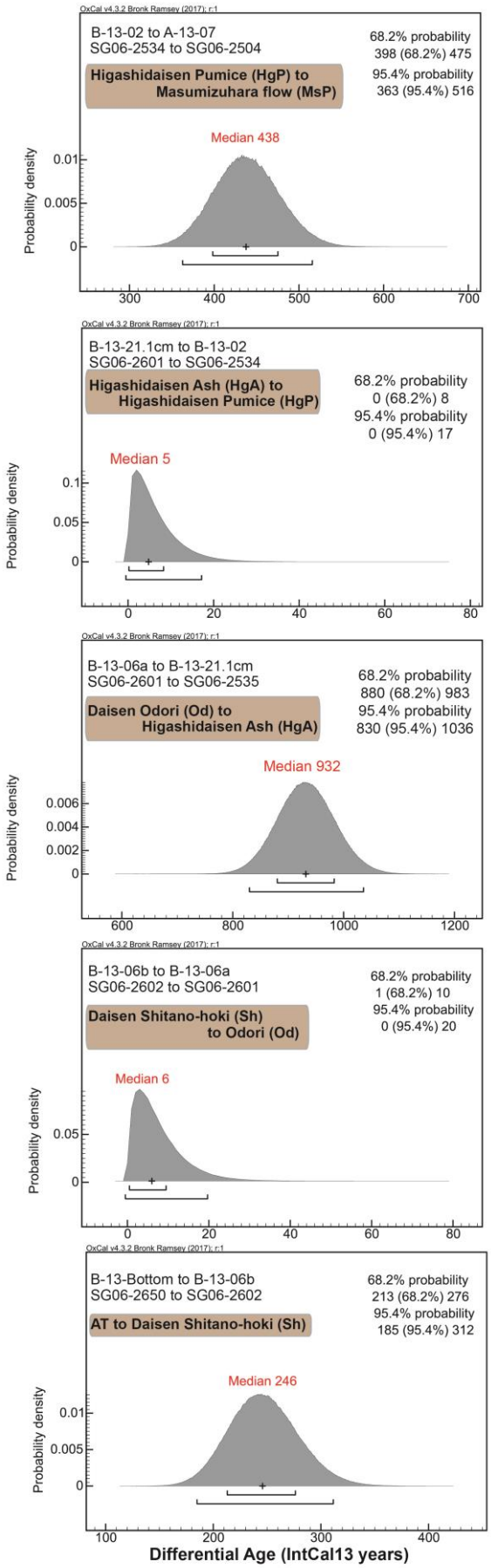

Supplementary Figure 3

1229